Environmental Earth Sciences (2023) 82:420
https://doi.org/10.1007/s12665-023-11083-y

ORIGINAL ARTICLE

Orogenic lode-gold deposits and listvenization processes in the El-Barramiya area, Eastern Desert, Egypt

Mohamed Abdelrady[1] · Hany Elhadek[1] · Mohamed Abdelmoneim[1] · Ahmed Saleh[2]

Received: 11 March 2023 / Accepted: 29 July 2023 / Published online: 24 August 2023

Abstract

Gold mineralization in the El-Barramiya region of the Eastern Desert, Egypt, is connected to the post-accretionary stage throughout the Central Eastern Desert. It is represented by quartz, quartz-carbonate veins and disseminations in listvenite rocks. The thrust contact between rock units in El-Barramiya area played an imperative part in gold mineralization where the obduction of ophiolitic rocks over the metasediments and metavolcanics caused shear zones. Mineralization in the study area formed along shear zones and the gold mineralization prefers to precipitate along the transition zone between low-grade regional metamorphic area which is represented by metasediments and high grade which is represented by actinolite schist. The gold mineralization lode of El-Barramiya gold mine area is situated in E–W trending quartz and quartz-carbonate veins along a shear zone located in the intersections between faults trend in NE–SW (Najd fault), NW–SE and thrust faults trend in NEE–SWW in metavolcanic and metasedimentary host rocks. Porphyry granite in the mine area played an important role in hydrothermal alteration process where it represents the source of K, listvenite formed when fluids rich in CO_2 and bearing-K permeate and alter the previously altered ultramafic rocks, usually serpentinites of the ophiolitic mélange rocks. The listvenitization process includes silicification and carbonatization metasomatic processes, tectonized serpentinites are altered to listvenite as the carbonatization becomes more intense close to dipping transpressive faults. Geochemical studies of listvenite and mineralized veins helped to determine the ultramafic genesis of listvenite and gold transformed as gold bisulfide. The whole rock geochemical data from El-Barramiya and elsewhere indicate that the transformation of serpentinite into listvenite involves profound metasomatic modification of the bulk-rock geochemistry. The chemical changes during alteration of serpentinite to listvenite are dominated by the addition of CO_2, the removal of H_2O, and the redistribution of SiO_2, MgO and CaO as carbonate minerals and silica replace serpentine. All listvenites at El-Barramiya lode gold deposit are enriched in CaO, Fe_2O_3 and K_2O, but depleted in MgO compared with associated serpentinite that is presumed to represent their protoliths. The chemical changes during alteration of serpentinite to listvenite are dominated by the addition of CO_2, the removal of H_2O, and the redistribution of SiO_2, MgO and CaO as carbonate minerals and silica replace serpentine. Alteration also caused redistribution of trace elements, with some being locally remobilized within the rock, some being added from a fluid phase, and others being leached out of the rock. Petrographic investigation and geochemical studies show different types of alterations (carbonatization and silicification) and mineralization. Mineralizations are represented by gold and sulfides (pyrite, arsenopyrite and smaller quantities of chalcopyrite, sphalerite, galena, tetrahedrite and gersdorffite) found in auriferous quartz veins and disseminated in listvenite. The area exposed to brittle–ductile deformation in addition to different types of structures such as faults and fractures controlling on the formation of mineralization and act as hydrothermal channels ways for fluid flow. Fluid inclusions studies revealed that gold mineralization was formed from heterogeneous trapping of H_2O–CO_2 fluids at a temperature of 280–340 °C and pressure within the range of 1.5–1.9 kbar, which is consistent with the mesothermal conditions.

Keywords Orogenic gold · Listvenite · Mineralized veins · Sulfides · Mineralizing conditions

Extended author information available on the last page of the article

Introduction

Orogenic gold deposits in collisional or post-collisional tectonic settings form via a range of transpressional to compressional processes (Groves et al. 1998; Goldfarb et al. 2001). Such deposits commonly exhibit the following characteristics: (1) their host rocks are deformed and metamorphosed, although mineralization is structurally controlled by brittle faults or ductile shear zones that cross-cut metamorphic fabrics; (2) fluid inclusions indicate the presence of low-salinity ore-forming fluids that are primarily mixtures of H_2O and CO_2, with minor CH_4 and N_2, and a near-neutral pH; (3) associated metasomatic alteration assemblages contain quartz, sericite, sulfide, carbonate, and chlorite (Chen 2006; Goldfarb et al. 2001; Groves 1993; Groves et al. 1998; Pirajno 2009). Thermobarometry performed on these deposits indicates that the mineralized lodes formed at pressure–temperature (*P–T*) conditions of 1–5 kbar and 200–650 °C, representative of the upper and middle continental crust.

The Arabian-Nubian Shield (ANS) is a developing world-class area for gold assets where gold deposits are broadly linked to post-tectonic granitoid rocks (El-Gaby et al. 1988; Pohl 1988). Gold is common within Egypt's Eastern Desert, with major deposits identified in El Sukkari, Hamash, and El-Barramiya. According to Goncharenko (1970) and Kuleshevich (1984), the term "listvenite" was first used by Soviet geologists in the Ural goldfields of Russia and is now commonly used throughout Europe and North America. It defines a mineralogical assemblage that emerges from the carbonatization of serpentinized ultramafic rocks and represents a peculiar alteration suite that is frequently connected to quartz-carbonate lode gold deposits. Listvenite forms when fluids rich in carbon dioxide permeate and bearing K alter the previously altered ultramafic rocks, usually serpentinites. Although listvenite has long been known to exist in Saudi Arabia's Neoproterozoic rocks, several of these occurrences have recently undergone fresh research due in large part to its close connection to gold mineralization (Gahlan et al. 2020a, 2022). Carbonation causes the destabilization of the silicates, minor oxides, and sulfides that make up serpentinized peridotites, affecting the redistribution of transitional elements between minerals and fluids. The carbonation of listvenite is accompanied by changing assemblages of Fe oxides and sulfides in Fanja (Decrausaz et al. 2023). An important geological process having significance for the production of ore deposits is carbonatization of mafic–ultramafic rocks (Gahlan et al. 2020a; Moussa et al. 2021). In addition to sulfides and other hematite, magnetite, cobalt minerals, and chromite remnants, listvenite frequently contain quartz, carbonate minerals (magnesite, ankerite, and dolomite), and/or fuchsite. According to Osman (2014), El-Barramiya is considered one of the deposits related to Mubarak-Hamash structural block. El Barramiya gold mine area is located at the intersection zone between two major shear zones trending E–W and NW–SE directions (Fig. 1C). The Intersection zones promoted gold mineralization of gold because this area becomes highly sheared due to the effect of brittle–ductile deformation and also the porphyry granite played an important role in hydrothermal solutions and listvenitization process (Zoheir and Lehmann 2011). Buisson and Leblanc 1986; Likhoidov et al. 2007 stated that granitic magmatism has a role in the development of the most fruitful listvenite-related gold resources. The area contains different types of structures such as faults, joints, and foliations (Fig. 1A, B, E).

El Barramiya gold mine area is located at the intersection zone between two major shear zones. The early shear zone trending E–W due to obduction of serpentinite on metasediments and metavolcanics and the later is Najd shear zone which trending NW–SE. The area has become highly sheared due to the effect of brittle–ductile deformation and also the porphyry granite played an important role listvenitization process, and this has resulted in deposition of gold in the intersection zones (Zoheir and Lehmann 2011). Buisson and Leblanc 1986; Likhoidov et al. 2007 stated that granitic magmatism has a role in the development of the most fruitful listvenite-related gold resources.

El-Barramiya area has been studied by many researchers in order to identify subsurface structures, such as faults, shear zones, and lithological contacts, which may affect ore deposit mineralization and allow effective prospecting via a range of geological and geophysical techniques (Mahmoud et al. 2013; Saleh et al. 2018; Mohamed et al. 2022; Abdelrady et al. 2023). Here, we present the results of field work (Fig. 1), petrography, fluid inclusion analysis, and geochemical analyses of mineralized rocks (listvenites, and gold-bearing quartz and carbonate veins) in the El-Barramiya area. From these new data, we interpret the source of the auriferous fluids that led to ore formation, constrain the physico-chemical conditions of mineralization, and identify the major structural controls on the mineralization of ore deposits. The present study covers the applications and importance of fluid inclusion technique, geochemical data for tracing origin of ore-forming fluids, the source of gold and transporting form of Au.

Geological setting

Depending on substantial contrasts in physiographic characteristics and exceptional variances in exposed lithologies, the Eastern Desert of Egypt can be divided into three

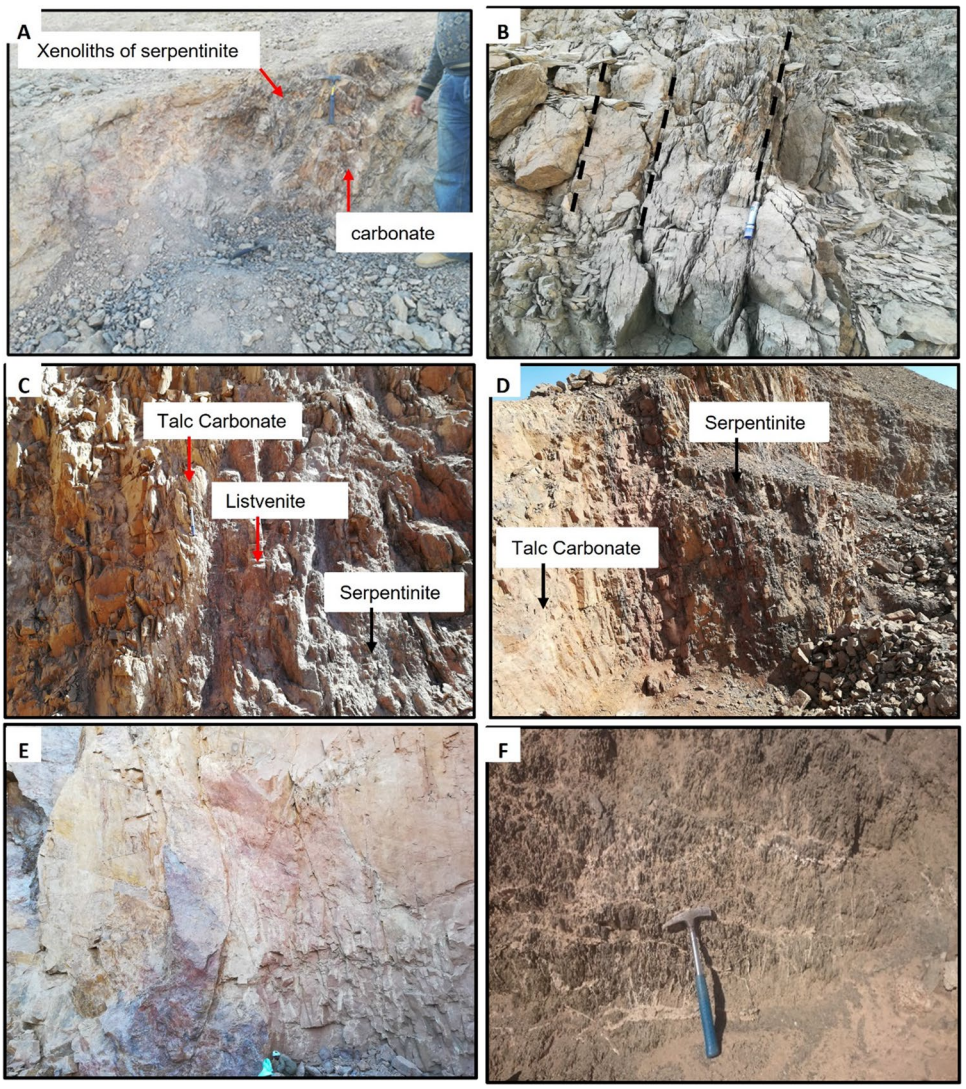

Fig. 1 Field relationships at the Barramiya mine area. **A** Xenoliths of Serpentenite in carbonate rocks, **B** foliation (N75° E–S255° W) best preserved in the actinolite–tremiloite schist adjacent to the tectonized serpentinites. **C** Highly sheared alteration zone for mineralization in the study area. **D** Foliation of talc carbonate and serpentinite in the E–W direction (**E**) Joints in listvenite rocks in the study area. **F** Highly shared serpentine with stockwork vienlets of carbonate

main provinces; the Northern Eastern Desert (NED), the Central Eastern Desert (CED), and the Southern Eastern Desert (SED) (Abdel Khalek 1979; El-Gaby et al. 1988; Stern and Hedge 1985; Fowler and Osman 2009). The provinces are arranged in opposition to one other along two important structural elements: the Idfu-Mersa Alam Shear Zone separates CED from SED and the Qena-Safaga Shear Zone separates NED from CED. The El-Barramiya region is located in the western portion of the CED, near to its boundary with the SED. The area is located between longitudes 33° 45′ E and 33° 55′ E and latitudes 25° 00′ N and 25° 10′ N and covers about 65 km^2 in surface area and is considered a part of the Arabian Nubian shield (Fig. 2C). The basement rocks of El-Barramiya is represented by dismembered ophiolite fragments obducted on metasediments and metavolcanic. During pan-African (Pre-Cambrian) serpentinites were obducted onto island arc metavolcanic and metasedimentary rocks, which themselves are intruded by deformed gabbro and diorite (Fig. 2A).

Later, subduction related to syn-continental, calc-alkaline, and syn-orogenic granitoids related post- continental collision intruded across this entire sequence, and post-orogenic granites (monzogranite and porphyry) occur in the northern and southern parts of the study area. The study area is also cross-cut by dykes of basic to acidic composition. These ophiolitic mélange rocks in El-Barramiya area are covered from the western part the Nubian Sandstone, which is Upper Cretaceous and Cambrian in age and this resulted in unconformity between basement rocks and sedimentary rocks (Fig. 2A).

Along the thrust zones, talc, magnesite and chromite form veinlets, nodules or irregular pockets are occupied in the sheared ultramafic rocks (Fig. 1D, C, F). Tectonized serpentinites (Fig. 1D, C) such as talc-actinolite schist and talc carbonate rocks are altered to listvenite as near

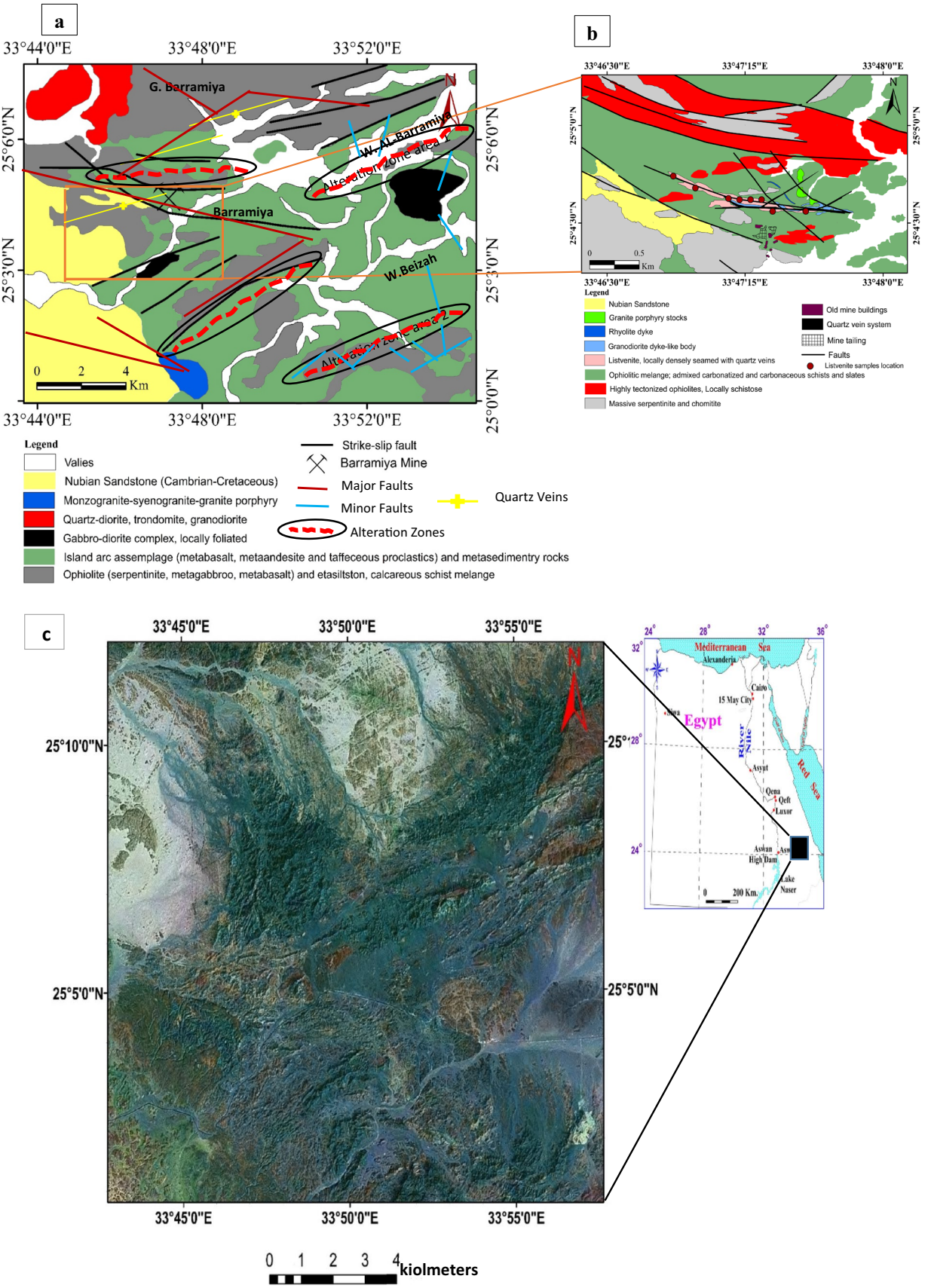
a
33°44'0"E
33°48'0"E
33°52'0"E
25°6'0"N
25°3'0"N
25°0'0"N
G. Barramiya
W. AL Barramiya
Alteration zone area 1
Barramiya
W.Beizah
Alteration zone area 2
N
0 2 4 Km
b
33°46'30"E
33°47'15"E
33°48'0"E
25°5'0"N
25°4'30"N
0 0.5 Km
Legend
Nubian Sandstone
Granite porphyry stocks
Rhyolite dyke
Granodiorite dyke-like body
Listvenite, locally densely seamed with quartz veins
Ophiolitic melange; admixed carbonatized and carbonaceous schists and slates
Highly tectonized ophiolites, Locally schistose
Massive serpentinite and chomitite
Old mine buildings
Quartz vein system
Mine tailing
Faults
Listvenite samples location
Legend
Valies
Nubian Sandstone (Cambrian-Cretaceous)
Monzogranite-syenogranite-granite porphyry
Quartz-diorite, trondomite, granodiorite
Gabbro-diorite complex, locally foliated
Island arc assemplage (metabasalt, metaandesite and taffeceous proclastics) and metasedimentry rocks
Ophiolite (serpentinite, metagabbroo, metabasalt) and etasiltston, calcareous schist melange
Strike-slip fault
Barramiya Mine
Major Faults
Minor Faults
Alteration Zones
Quartz Veins
c
33°45'0"E
33°50'0"E
33°55'0"E
25°10'0"N
25°5'0"N
Mediterranean Sea
Alexanderia
Cairo
15 May City
Egypt
River Nile
Red Sea
Aswan High Dam
Lake Naser
0 200 Km.
0 1 2 3 4 kiolmeters

◂**Fig. 2** **A** Geological and structural map of the El-Barramiya area, **B** simplified geologic map of the El-Barramiya gold mine area after Zoheir and Lehmann (2011) and Zoheir and Weihed (2014). **C** Satellite image (ETM) showing the location map of the study area

steeply dipping transpressive faults, carbonatization intensifies. According to Zoheir and Lehmann (2011) listvenite is represented by a several hundred meters long and elongate body up to 100 m broad near the mine area (Fig. 2B).

Several gold provinces have regional metamorphic profiles that show moderate to strong geothermal gradients during gold mineralization. There has been discussion on the genesis of gold lodes and the connections between mineralization, metamorphism, and granitoid magmatic processes ever since the discovery of the Sukhoi lode gold–quartz–sulfide dispersed ore in 1961 (Buryak 1982). In El-Barramiya area, the coexistence of actinolite and chlorite in the peak assemblage, for example, suggests that the metamorphism only reached the greenschist-amphibolite facies transition, although Abu-Alam and Hamdy (2014) recommended upper greenschist facies (300–400 °C) for the ophiolitic rocks of the Arabian-Nubian Shield. The gold-bearing quartz and quartz-carbonate veins are geographically and chronologically connected to a dextral shear system that formed in the area during late phases of its deformation history (See Zoheir and Lehmann 2011). Petrographically, large and severely asymmetric and distorted microstructures, dynamic recrystallization, and slip on discrete carbonaceous laminae suggest that the mineralized quartz veins formed from a variety of compressional and tensional regimes (cf. Cox et al. 1987).

Methods

Petrographic studies

Petrographical study where more than 100 thin sections from different rock units include country rocks and quartz Veins have been investigated by the Zeiss optical polarizing microscope model Axioskop 40 for transmitted and reflected light to determine the textures and modal mineralogy of the samples in addition to Ore Microscopy for polished sections. Microscopic and scanning electron microscope (SEM) investigations of samples from mineralized quartz veins with visible areas of sulfide minerals helped to establish a paragenetic sequence of ore minerals. Samples with interesting microscopic features observed by optical microscopy at the geology department, faculty of science, University of Assiut.

Geochemical studies of listvenite and quartz vein rocks

Fourteen samples have been analyzed for major, trace and rare earth elements. Eight samples from listvenite rocks and six samples from hydrothermal quartz veins. These analysis were carried out using ICP-MS technique at ACME laboratories in Canada. SiO_2 and LOI were analyzed using gravimetric method in the geochemistry lab, faculty of science, Assiut University. Bulk chemistry analysis have been done on selected samples using AQ250–Ultratrace by ICP Mass where the detection limit equal 1 ppm for 15/30 gm analysis for 37 elements. Double-polished wafers 200–300 µm thick were prepared from the samples.

Fluid inclusion studies of listvenites and quartz veins

Double-polished wafers 200–300 µm thick were prepared from the samples. The present study includes the genetic and non-genetic description of fluid inclusions as well as the phase transition (microthermometry). Microthermometric runs were carried out at the Geology Department, Faculty of Science, Assiut University using a Linkam THMS 600 heating/freezing stage. The stage was calibrated for temperatures between − 56.6 and + 400 °C using Merck chemical standards as well as according to the melting point of distilled water (0 °C) and phase transition in natural pure CO_2 inclusions with triple point at (− 56.6 °C). From microthermometric results, the bulk composition and density of the fluids are calculated by using the equation of state of Zhang and Frantz (1987) for H_2O–NaCl system and Brown and Lamb (1989) for volatile-rich system. Isochores for different fluid densities are calculated until a fit with the known homogenization temperature is achieved using FLINCOR computer program (Brown 1989). The minimum pressure of trapping is estimated from the constructed P–T diagrams.

Relationship between gold mineralization and metamorphism

Several gold provinces have regional metamorphic profiles that show moderate to strong geothermal gradients during gold mineralization. There has been discussion on the genesis of gold lodes and the connections between mineralization, metamorphism, and granitoid magmatic processes ever since the discovery of the Sukhoi lode gold–quartz–sulfide dispersed ore in 1961 (Buryak 1982). In El-Barramiya area, the coexistence of actinolite and chlorite in the peak assemblage, for example, suggests that the metamorphism only reached the greenschist-amphibolite facies transition, although Abu-Alam and Hamdy (2014) recommended upper

greenschist facies (300–400 °C) for the ophiolitic rocks of the Arabian-Nubian Shield. The gold-bearing quartz and quartz-carbonate veins are geographically and chronologically connected to a dextral shear system that formed in the area during late phases of its deformation history (See Zoheir and Lehmann 2011). Petrographically, large and severely asymmetric and distorted microstructures, dynamic recrystallization, and slip on discrete carbonaceous laminae suggest that the mineralized quartz veins formed from a variety of compressional and tensional regimes (cf. Cox et al. 1987).

Hydrothermal alteration processes

According to Hansen et al. (2005), serpentine minerals decompose into magnesite and talc due to carbonization, producing water. As alteration progresses, the silica content increases at the expense of carbonate and produces listvenite, which is a silica- and carbonate-rich mineral. The following petrographic descriptions document hydrothermally altered serpentinites samples from the El-Barramiya area.

Listvenite

Listvenite is a fine-to medium-grained rock that has reddish or yellowish-brown colors in hand sample. In the El-Barramiya area, samples either have a mylonitic schistose texture created by shearing, while others are porous. Petrographically, listvenite is mostly made up of magnesite (40–60 vol%), quartz (30–50 vol%), dolomite (5–10 vol%), and fuchsite (chromian muscovite), with minor serpentine, Cr–spinel remnants, and sulfide minerals. Reactions (1, 2) produce different generations of magnesite (M1, M2 and M3) (Hansen et al. 2005):

$$\underset{\text{Antigorite}}{2\,Mg_{48}Si_{34}O_{85}(OH)_{62}} + 45\,CO_2 \rightarrow \underset{\text{Magnesite + Talc + Water}}{45\,MgCO_3 + 17\,Mg_3Si_4O_{10}(OH)_2 + 45\,H_2O}, \quad (1)$$

$$\underset{\text{Talc}}{Mg_3Si_4O_{10}(OH)_2} + 3\,CO_2 \rightarrow \underset{\text{Magnesite + Quartz + Water}}{3\,MgCO_3 + 4\,SiO_2 + H_2O}. \quad (2)$$

Quartz in weakly deformed listvenite appears as strongly deformed amorphous crystals with a colloformal structure and as coarse isolated wedges. Amorphous microbands of quartz (chalcedony) also occur. Fuchsite in weakly deformed listvenite occurs as fine flakes of green color associated with carbonates, thin bands and cavity fillings (Fig. 3F–H).

Highly sheared mylonitized listvenite

Strongly sheared listvenite consists of distinct greenish grey, reddish-brown carbonate-quartz bands with foliated mafic–ultramafic microlithon bands (fuchsite, quartz, and chlorite) (Fig. 3A). Altered asymmetric C/S, C' fabrics, and S-style (winged) magnesite porphyroclasts bounded by fuchsite veinlets are also present. Increased shear strain is manifested by bended flakes of the mica fish elongated parallel to the direction of lineation. Asymmetric S-style quartz–carbonate veinlets are recorded. Common hydrothermal veins of quartz and quartz–carbonate with gold and sulfides mineralization fill these micro-cracks and fractures. Listvenite shows evidence of both brittle and ductile deformation. The change from compression to extensional deformation in the listvenite is manifested by S-shape sigmoidal tension gashes that formed along ductile shear zone (Fig. 3B). The early generation M1 exhibits a euhedral outline with respect to serpentine relics. It is often stained with iron oxides and variably deformed. With shearing progress, M1 is overgrown by dark color M2 magnesite associated with talc (Fig. 3G). The dark color may be due to higher in the Fe. The latest generation of magnesite M3 is represented by carbonates veinlets and veins filling the fractures in the highly sheared mylonitic listvenite. The M3 Magnesite associated with quartz, dolomite and calcite.

Quartz and quartz–carbonate veins

Three generations (V1, V2 and V3) (Fig. 4A–C) of quartz and quartz–carbonate veins can be recognized in the area of study. Their length ranges from 70 to 300 m, and their widths range from 10 cm to 1 m. The first and pre-mineralization stage (V1) is generally milky white, lacks Au- and sulfides, and developed along regional schistosity (ENE–WSW). An assemblage of carbonate, graphite, fuchsite ± chlorite minerals occupy the serrate planes separating bent quartz crystals, producing a distinctive stylolitic texture (Fig. 3C). Mineralized veins (stage V2), contain Au and sulfides, and have thicknesses up to 15–20 cm. They are connected to E–W shear zones, related fractures and anastomosing zones. Asymmetric structures (e.g. C/S or C' shear bands) as well as intrafolial asymmetric folds document the V2-stage (Fig. 3D), indicating that V2-stage quartz veins are related to low-grade mylonitic shear zones. In certain veins, magnesite–siderite ± calcite aggregates and fibres fill the open vugs as replacement phases and are connected to comb quartz. Post-mineralization stage (V3) veins in sharply sloping NW–SE extensional cracks are barren, contain milky white quartz, and are aligned parallel to the Najd fault system.

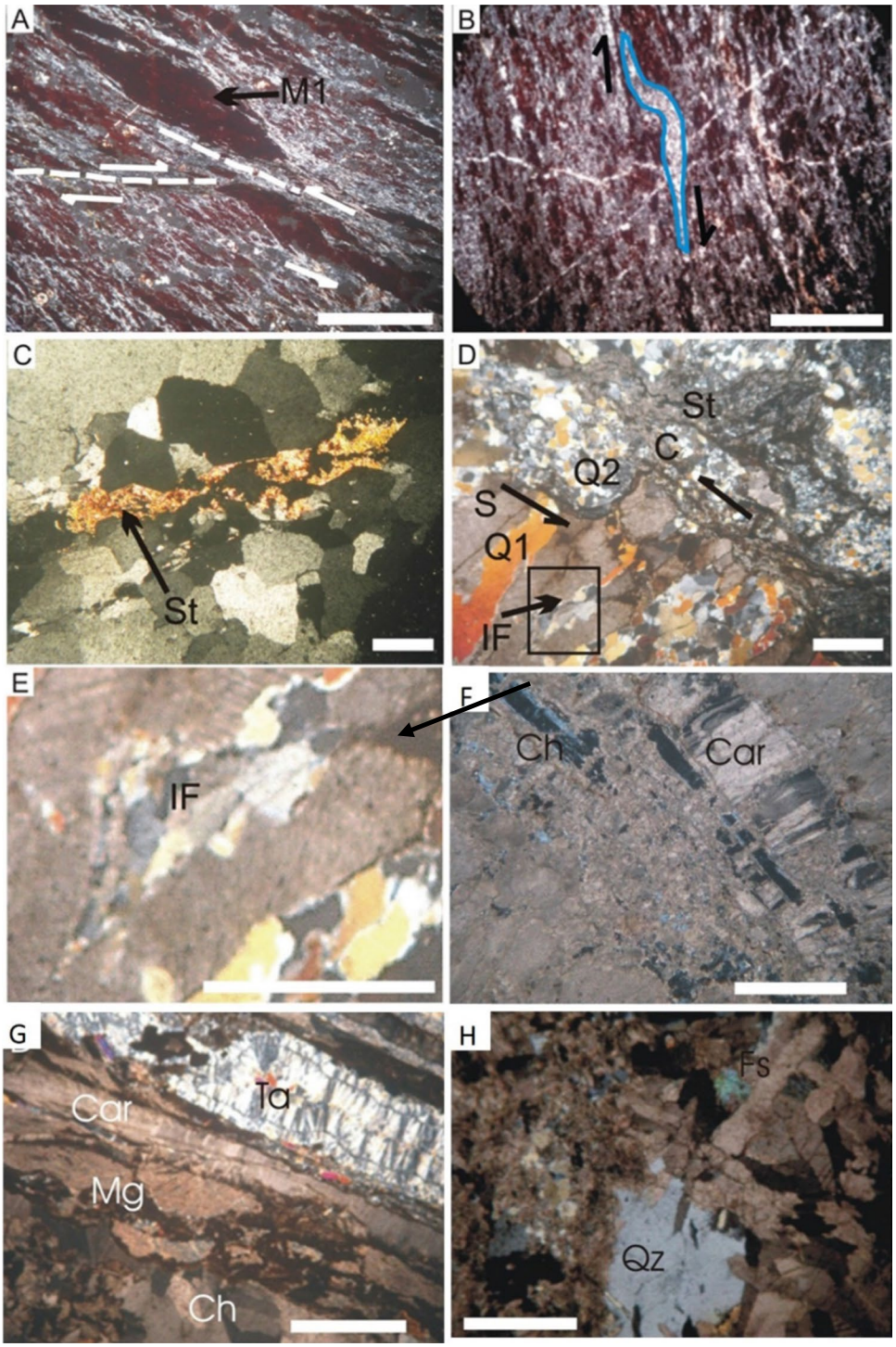

Fig. 3 Photomicrographs show: **A** Mafic microlithon bands (quartz and chlorite), reddish brown carbonate-quartz bands in sheared mylonitic listvenite, an augen shape of coarse grained magnesite crystals and asymmetric microstructure C/S. M1 is characterized by euhedral outline of early formed magnesite. **B** S-shape sigmoidal tension and gashes form along ductile shear indicating extensional deformation. Arrows show the direction of movement. **C** Carbonate stylolitic texture indicates ductile deformation of quartz of V1 stage. **D** Carbonates stylolitic structure (St), C/S and C' asymmetric fabrics and intrafolial asymmetric folds (IF) as well as recrystallized quartz (Q2) as indication to ductile shear deformation. **E** Enlargement of intrafolial asymmetric folds in **D**. **F–H** Photomicrographs of ore minerals associated with listvenite, quartz and quartz – carbonate veins. **G** Banded and brecciated talc carbonate, and the early appearances of amorphous quartz (Ch). **H** Carbonate rich listvenite, cavity filling quartz (Qz) and fushsite (Fs). **F** Alternate bands of carbonate (Car) and amorphous quartz (Ch). The latter is also present as filling microfractures in the carbonate bands. Bar 200 µm

Ore minerals

The ore mineral concentrations in the El Barramiya gold mine area ranges from 1.6 to 7.5% of the rock volume (Abdel-Karim et al. 2017). They are represented by sulfides, chromite, magnetite, hematite and gold. Both gold and sulfides ore minerals occur scattered throughout the quartz, quartz carbonate veins and adjacent wall rocks. They are most prominently represented by arsenopyrite, pyrite and trace amounts of chalcopyrite, sphalerite, tetrahedrite, galena, pyrrhotite, gersdorffite and gold. Secondary minerals include covellite and goethite. According to Zoheir and Lehmann (2011) sulfides are typically less than 2% of the vein volume, but their abundance varies along the vein's breadth. In listvenite and schist adjacent to the veins, sulfides occur as scatter disseminations (Fig. 5H). In quartz

Fig. 4 Field photographs show the characteristics of different types of quartz veins in El-Barammiya gold mine area. **A** Stage V1 pre-mineralization highly deformed, boudinaged and cataclsites quartz veins parallel to the main foliation trend of the study area. **B** Fissure filling mineralized quartz–carbonate veins (stage V2). These veins are micro-brecciated, slip and bounded by carbonatized graphite- actinolite schist and listvenite. **C** Post mineralization veins (stage V3) intersected the brecciated V2 and F3 folds

and quartz carbonate veins, gold and sulfides mineralization are restricted to the stylolitic planes in recrystallized quartz veins, where disseminated sulfides are associated with a carbonaceous material (Fig. 5I). The early generation granulated and brecciated quartz are enclosed in a network of carbonate. Arsenopyrite and pyrite are the principal hosts of submicroscopic gold, where very fine-grained inclusions (~ 10 µm) of gold are detected within margins of pyrite and arsenopyrite crystals. It also occurs as minute crystals (up to 20 µm) either disseminated in the carbonates (Fig. 5I) or distributed along healing microfractures of quartz crystals (Fig. 5G). Under reflected light microscope, arsenopyrite is characterized fine- to medium-grained (30–500 µm), silvery-white to steel gray. Arsenopyrite is characterized by weak

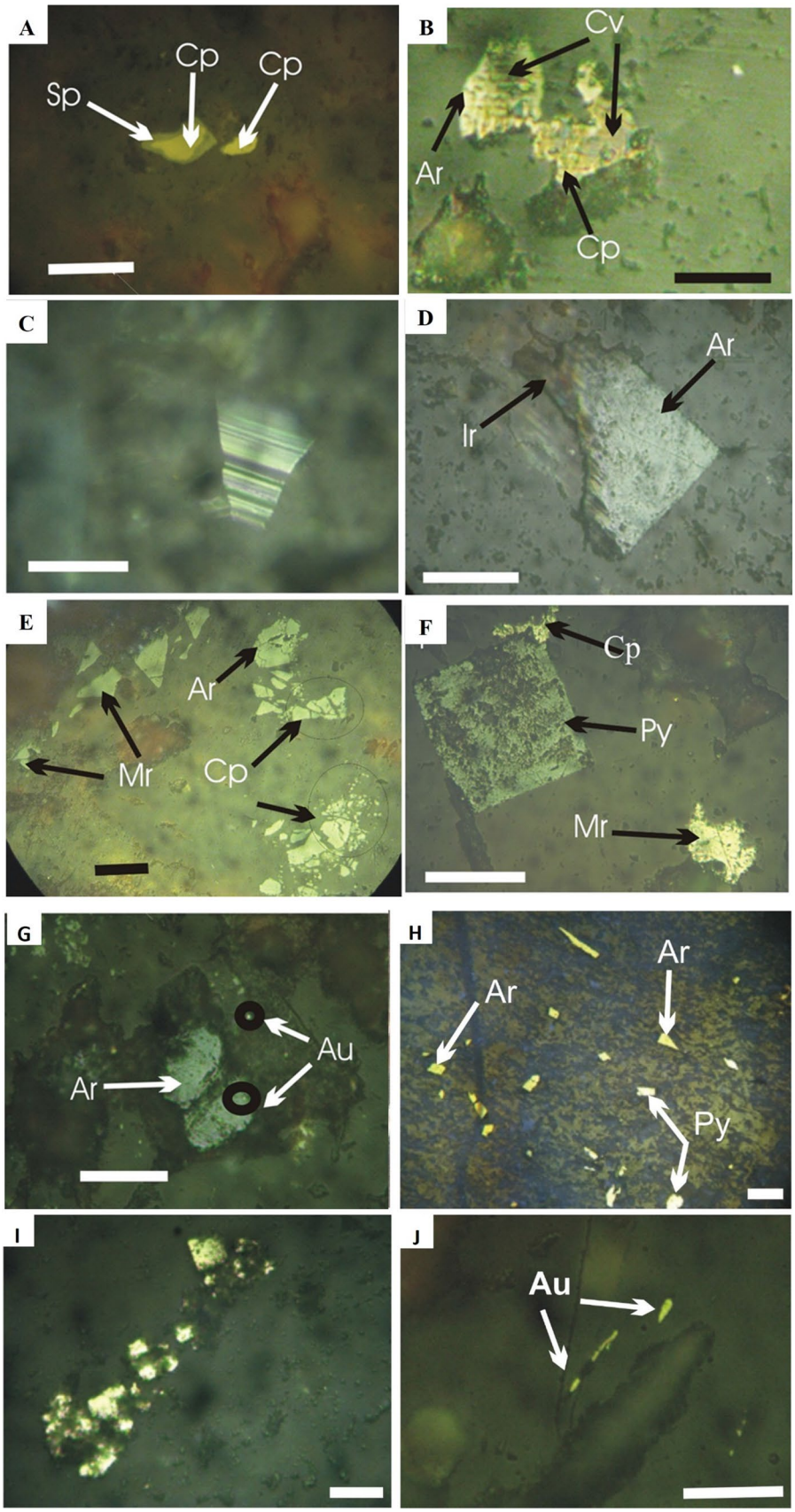

Fig. 5 **A** Chalcopyrite (Cp) crystal replaced by sphalerite (Sp) along the margins. **B** Large crystal of arsenopyrite (Ar) replaced by chalcopyrite (Cp), which altered to covellite (Cv). **C** Twinned arsenopyrite (001) in the listvenite from wall rock. **D** Iridescent colors (Ir) of the oxidized arsenopyrite crystal (Ar). **E** Highly deformed and cataclastic large crystals of pyrite (Py) in associated with arsenopyrite and marcasite. **F** Chalcopyrite (Cp) replacing large crystal of pyrite (Py), and associated with marcasite (Mr). **G** Iridescent colors (Ir) of the oxidized arsenopyrite crystal (Ar). **H** Disseminated arsenopyrite (Ar) and pyrite (Py) in listvenite country rocks. **I** Disseminated arsenopyrite and pyrite along stylolitic carbonate structure planes in quartz veins. **J** Fine-grained grains of gold (Au) arranged parallel to stylolitic carbonate plane. Bar 200 µm

pleochroism from white or bluish tint, faint reddish yellow and strong anisotropism (red-violet). Crystals of arsenopyrite with common twinning on (100) are detected (Fig. 5C). It is easily oxidizing to slightly iridescent colors of pink, brown, or copper (Fig. 5D). Very fine-grained inclusions (~ 10 µm) of gold is detected in or within marginal to pyrite and arsenopyrite crystals (Fig. 5B). Gold is characterized by yellow color, non-pleochroic and none internal reflections. Marcasite is commonly recorded as pseudomorphism of cracked and cataclasites large pyrite crystals in association with chalcopyrite and digenite (Fig. 5E, F). Marcasite does not have the same brassy yellow color of pyrite. Instead, it is a pale brass color. Chemical analysis of pyrite after Zoheir and lehmann (2011) using electron microprobe proved the presence of traces of Ni (up to 0.69 wt%), As (up to 0.67 wt%), Cu (up to 0.61 wt%) and occasional hundreds of ppm Au.

XRD identification of listvenite rocks and quartz veins rocks

Mineralogical identification of the collected samples was performed using XRD at the physics department in Assiut University, Assiut. XRD analysis illustrate quartz, magnesite, dolomite and calcite are the most common minerals in listvenite rocks where the principal peaks of *quartz* are indexed with their d-spacing and relative intensities, as follows: 20.671° 4.297 Å; 20.808° 4.269 Å; 26.582° 3.353 Å; 26.591° 3.352 Å; 54.88° 1.673 Å; 54.82° 1.675 Å; 59° 1.501 Å. *Magnesite* follows the quartz in abundance and is where the principal peaks appears 42.424° 2.131 Å; 42.28° 2.138 Å; 32.439° 2.76 Å; 44.56° 2.033 Å; 44.892° 2.019 Å; 54.892° 1.673 Å; 59° 1.501 Å. *Dolomite* is represented on the XRD charts by the characteristics lines at d-spacing and relative intensities 30.797° 2.903 Å; 30.878° 2.896 Å; 33.46° 2.678 Å; 35.868° 2.504 Å; 50.158° 1.819 Å; 51.018° 1.79 Å; 59° 1.501 Å. *Calcite* is represented on the XRD charts by the lines at d-spacing 3.137 Å, 2.418 Å, 2.335 Å and 3.037 Å and relative intensities 28.454°, 37.18°, 38.56° and 29.414°. Iron oxides are represented by chromite, hematite and magnetite (Fig. 6A, B). *Chromite* is represented on XRD charts by d-spacing 2.986 Å and 4.745 Å and relative intensity 30.88° and 18.7°. Hematite is represented on XRD charts by d-spacing 2.284 Å and 2.24 Å and relative intensity 39.451° and 40.254°. *Magnetite* also represented on XRD charts by d-spacing 2.61 Å and relative intensity 34.36°.

XRD analysis indicate that quartz is the most abundant mineral in the studied rocks from d-spacings and relative intensities, as follows: 20.79° 4.272 Å; 26.555° 3.357 Å; 50.149° 1.819 Å; 36.515° 2.461 Å 20.732° 4.285 Å; 26.47° 3.367 Å. 36.448° 2.465 Å; 50.069° 1.822 Å 59.87° 1.545 Å.

Mineral association and paragenesis

The early oxide ore minerals in the studied area are represented mainly by chromite and magnetite. *Chromite* forms irregular to euhedral fractured crystals with silicate minerals filling the cracks. Moreover, cataclastic and brecciated chromites are recorded in talc-carbonate and carbonate rich listvenite rocks. *Magnetite* is mostly common in talc-carbonate, but also detected in listvenite rocks. It appears as anhedral crystals with peripheral granules of pyrite. Sulfides ore minerals disseminated in the quartz veins and adjacent wallrocks (listvenite and graphite schist) are mainly arsenopyrite, pyrite and smaller amounts of chalcopyrite, sphalerite, tetrahedrite, galena, pyrrhotite, gersdorffite and gold. Based on rock association alterations and textural relations (intergrowth and replacement), a two-stage mineralization paragenesis is suggested for the Barramiya deposit (Table 1). During the early mineralization stage, arsenopyrite, gersdorffite, pyrrhotite, pyrite ± refractory gold has been formed, followed by chalcopyrite, tetrahedrite, sphalerite, galena and free gold in the late mineralization stage. The bulk sulfide mineralization was overprinted by a late, variably pervasive secondary alteration which represented by marcasite, covellite, bornite goethite and hematite.

Fluid inclusions

Various kinds of fluid inclusions were noted in quartz-filling cavities and fractures in listvenite (Table 2), which include type-1 $H_2O–CO_2 \pm CH_4$ inclusions, type-2a ($H_2O + CO_2$) inclusions (Fig. 7A, B), type-2b two-phase (L–V) aqueous inclusions and type-3 secondary aqueous inclusions, which are represented by two-phase (L–V), mono-phase liquid and mono-phase vapor inclusions. In type-1 inclusions, the melting temperature ranges between − 70.2 and − 58.6 °C indicating the presence of CH_4-phase. Clathrate melting ($Tm_{clat.}$) ranges between 9 and 12 °C, indicating very low salinity < 3 wt% NaCl eq. (Diamond 1992; Fall et al. 2011). The homogenization temperature of CO_2 (Th_{CO2}) was achieved between 26 and 29 °C, corresponding to CO_2-density between 0.631 and 0.697 g/cm^3. Due to decrepitation, bulk homogenization was recorded in few inclusions between 360 and 390 °C. In type-2a inclusions, Tm_{CO2} was measured at temperatures between − 62 and − 57.2 °C, slightly below the triple point of CO_2, indicating the existence of trace quantities of dissolved components like CH_4, this was confirmed by laser Raman spectroscopy analysis (Zoheir and Lehmann 2011). CO_2-phases were homogenized to liquid between 20 and 25 °C, corresponding to densities of CO_2 (d_{CO2}) between 0.71 and 0.77 g/cm^3. The total homogenization

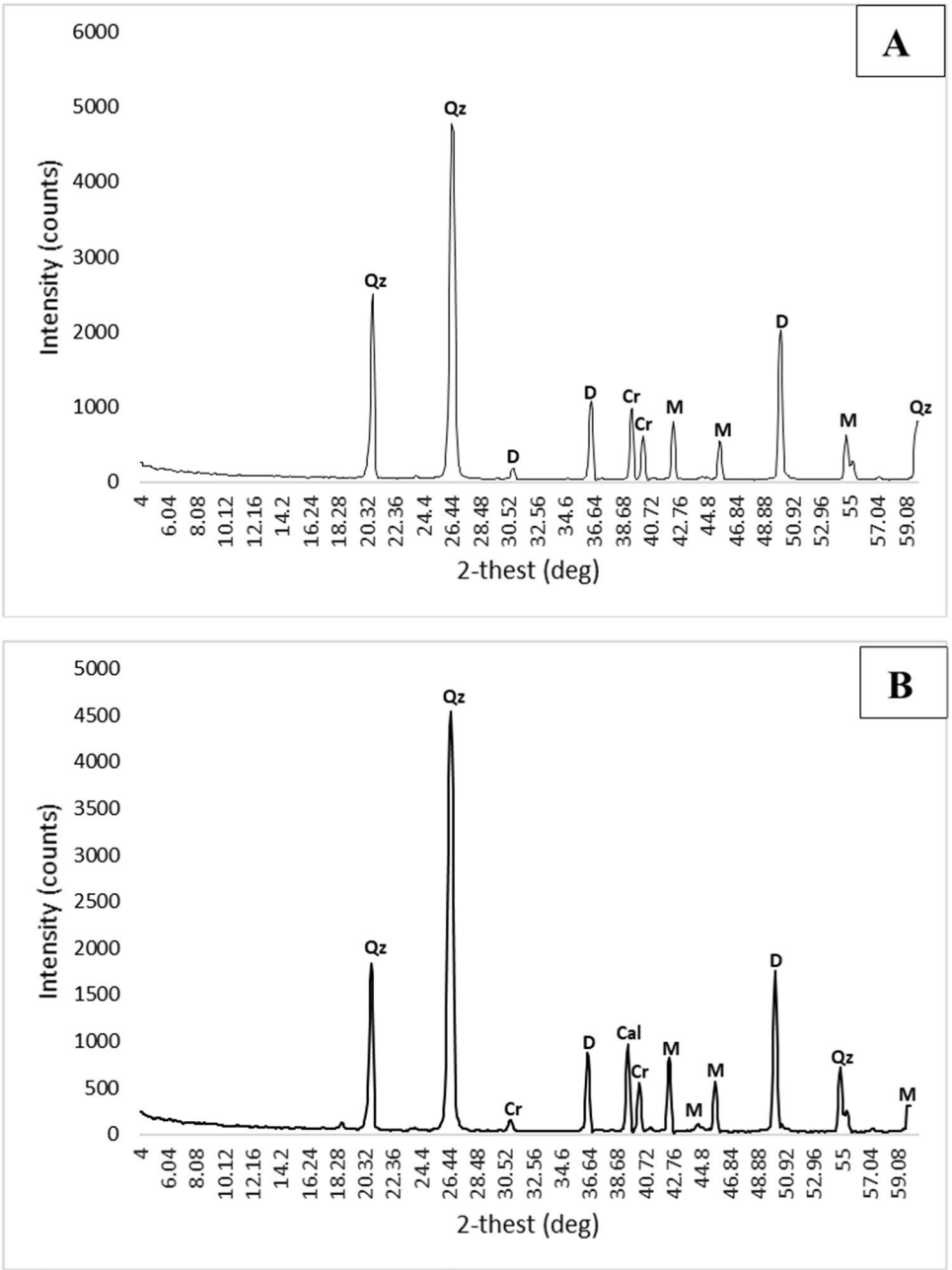

Fig. 6 **A**, **B** Photomicrographs showing the XRD charts of Listvenite rocks

temperatures were measured between 270 and 340 °C with a maximum peak at 300 °C (Fig. 7C). In type-2b inclusions, the total homogenization (Th_{tot}) to liquid was measured at temperatures ranging from 210 to 330 °C, with a peak at 280 °C (Fig. 7C). The trapping conditions, which represent the mineralizing conditions for gold and sulfides (arsenopyrite, pyrite, chalcopyrite, sphalerite, tetrahedrite, galena, pyrrhotite and gersdorffite) mineralizations, were characterized by temperature between 280 and 340 °C, and pressure between 1.5 and 1.9 kbar (Fig. 7D), which is consistent with mesothermal conditions.

Geochemistry

Major elements

Listvenite samples show wide variations in major oxide contents, which reflect the different degrees of metasomatic hydrothermal alteration of the precursor rocks in the study area. Two groups are distinguished based on their silica content: high-silica ($SiO_2 > 50$ wt%) and low-silica listvenites ($SiO_2 < 50$ wt%). All listvenites are enriched in As, Ni, Cr,

Table 1 Mineral association and paragenesis of ore minerals in El-Barramiya area

Rock type	Serpentinite	Talc Carbonate	Highly Sheared Talc Carbonate	Listvenite Carbonate-rich	highly sheared listvenite quartz Quartz -rich vein	quartz and carbonate
A. Oxides				Early-stage mineralization		late-stage min
Chromite						
Magnetite						
B. Sulfides and gold						
Gersdorffite						
Arsenopyrite						
Pyrite						
Chalcopyrite						
Shalerite						
Galena						
Tetrahedrite						
Gold						
Secondary hydrothermal minerals				Marcasite, covellite, bornite, goethite and hematite		

Table 2 Microthermometric results of fluid inclusions from the studied gold mineralization

Types of fluid inclusions	Microthermometric results
Type 1: H_2O–$CO_2 \pm CH_4$ inclusions	
Te	− 70.2 to − 58.6 °C
Tm_{clat}	9 to 12 °C
Salinity in wt% NaCl eq	< 3
Th_{CO2}	26 to 29 °C
Density (d_{CO2})	0.631 to 0.697 g/cm^3
$Th_{(tot)}$	360 to 390 °C
Type 2a: $H_2O + CO_2$ inclusions	
Tm_{CO2}	− 62 to − 57.2 °C
Th_{CO2L}	20 to 25 °C
Density (d_{CO2})	0.71 to 0.77 g/cm^3
$Th_{(tot)}$	270 to 340 °C
Type 2b: two-phase (L–V) aqueous inclusions	
$Th_{(tot)}$	210 to 330 °C

V, and Co, but have relatively low lithophile and other trace element/rare earth element levels (Table 3).

To understand the evolution of El-Barramiya listvenite, Harker diagrams were used to investigate co-variations of MgO with other oxides (Fig. 8). The figures show positive correlations with Fe_2O_3, CaO, and MnO, and negative correlations with alkalis (Na_2O and K_2O), Al_2O_3, SiO_2 and P_2O_5. Bivariate plots show negative correlations of SiO_2 versus MgO + CaO and Fe_2O_3 (Fig. 9A, B). The positive correlation of the loss of ignition (LOI) with MgO and MgO + CaO as well as the negative correlation with SiO_2 (Fig. 9C–E) infers that CO_2 in Mg-rich carbonates dominates the volatile component of the listvenites (see Gahalan et al. 2020a; b).

On SiO_2–Fe_2O_3–(MgO + CaO) ternary diagram, listvenite and average serpentinites from El-Barramiya plot along the SiO_2–(MgO + CaO) join (Fig. 10A). While some samples plot along the SiO_2–MgO solid line and others shift toward the SiO_2–CaO join on a SiO_2–CaO–MgO diagram (Fig. 10B). Therefore, the conversion of serpentinites to

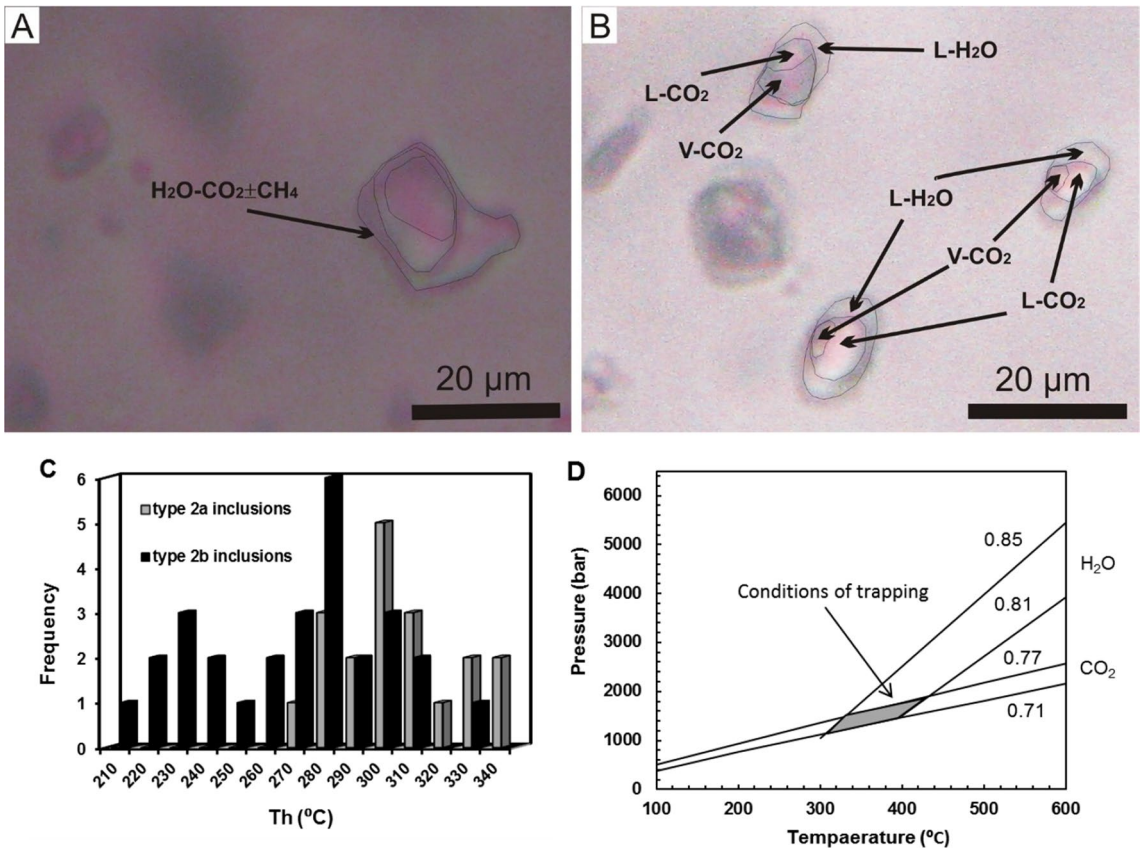

Fig. 7 **A**, **B** Photomicrographs show types, distribution and description of fluid inclusions at room temperature. **A** Primary distribution of type 1 (H_2O–$CO_2 \pm CH_4$) inclusions, **B** primary distribution of type 2a (H_2O–CO_2) inclusions in the mineralized veins, **C** histogram shows the total homogenization temperatures (Th) for type 2a and type 2b inclusions, **D** P–T diagram shows isochores of aqueous inclusions as well as CO_2-bearing inclusions

listvenite was accompanied by loss of MgO and gain of CaO and SiO_2, with progressive metasomatic alterations causing more and more extreme carbonatization and silicification. The gain of SiO_2 and loss of MgO with continued listvenitization of serpentinites also accounts for the negative correlation between SiO_2 and MgO on a SiO_2–MgO diagram (Fig. 10C).

Trace elements

Enrichment in Sr (47–770 ppm) and depletion in Ba (3–38 ppm) in listvenite compared to the average serpentinite (Table 3) may be attributed to the gain and loss of such elements, respectively, during metasomatism. Notably, the lowest Ni, Co and Cr concentrations were measured in the high-silica listvenite samples (5, 6, 7 and 8), In addition, the listvenite rocks contain higher (Ni, Co, and Cr) compared with quartz veins samples (Fig. 6A) can prove the ultrabasic origin of listvenite (Fig. 11A) (Table 4). The elements of Au, Ag, Cu, Sb, As, Rb, Ba, and Zn elements (Fig. 11B) in listvenite as well as quartz veins show random distributions. This random distribution reflects the overprint of metasomatic hydrothermal fluids on such elements. Both gold-bearing listvenite and quartz veins show similar positive correlations of Au and Ag contents with As, Cu, Zn, Pb, Sb and Tl (Fig. 12A, B). By contrast, Co, Ni, and Ba show different behaviors between mineralized quartz veins and listvenites: they show positive correlations in mineralized quartz veins and negative correlation in listvenite. These relations are consistent with petrographic observations showing that Au and sulfide mineralization is more common in late-stage (high-silica) listvenite, whereas base metal elements in low-silica listvenite are mostly barren. On the other hand, Au mineralization as well as other sulfides are disseminated in stylolitic carbonate and carbonates filling healed microfractures, which allow incorporation of base metals in the quartz-carbonate veins. Both listvenite and Au-bearing veins were subjected to brittle–ductile

Table 3 Major (%) and trace elements (ppm) and composition of the listvenite, serpentinites and quartz veins of El-Barramiya area

Sample no	Listvenite								Serpentinites	Quartz veins						
	1	2	3	4	5	6	7	8	(n=3)	9	10	11	12	13	14	
SiO_2	35.27	37.27	43.14	46.06	50.96	62.34	63.8	65.4	35.66	98.1	90.6	94.6	97.9	86.6	92.2	
Al_2O	0.585	0.226	0.056	0.075	0.075	0.623	0.151	2.985	0.91	0	0	0	0	0.11	0.68	
Fe_2O_3 (Tot.)	12.06	3.32	4.99	4.11	4.88	4.34	2.65	6.44	5.06	0.60	1.14	0.90	0.57	1.47	1.33	
MnO	0.193	0.187	0.059	0.076	0.107	0.391	0.076	0.028	0.083	0	0.02	0.02	0	0.03	0.025	
MgO	5.96	12.43	20.38	9.833	16.06	10.41	6.11	6.68	33.51	0.26	1.57	0.87	0.31	3.06	0.20	
CaO	15.02	22.02	5.37	15.19	5.302	4.23	10.87	0.78	2.7	0.43	2.47	1.3	0.34	5.16	1.93	
Na_2O	0.012	0.022	0.006	0.076	0.006	0.025	0.005	0.01	0.043	0	0	0	0	0	0.15	
K_2O	0.132	0.024	0.024	<0.01	<0.01	<0.01	0.072	<0.01	0.05	0.01	0.03	0.03	0.01	0.03	0.22	
P_2O_5	0.016	0.002	0.002	0.004	0.002	0.009	0.0068	0.112	0.013	0	0	0	0	0.01	0.109	
LOI	30.75	24.5	26.03	25.47	22.53	17.7	16.8	17.6	21.48	0.59	3.14	2.21	0.78	3.51	0.8	
Tot	99.99	100	100.05	100.8	99.93	100.06	99.93	100.03	99.53	99.99	98.97	99.93	99.91	99.98	97.64	
Ag(ppb)	0.095	0.153	0.008	0.032	0.015	0.119	0.968	0.078	Not analyzed	0.028	0.091	0.017	0.009	0.101	0.157	
As	856.6	1150.7	104.6	81.9	38.6	596.2	697.9	298.6	19.33	16.6	10	34	1.4	338.1	401.7	
Au(ppb)	0.825	0.220	0.0004	0.088	**0.047**	0.063	2.377	**0.0035**	Not analyzed	0.039	0.177	0.007	0.004	0.772	0.287	
Ba	13.9	7.8	38.3	14	2.5	12.1	7.3	19.7	38.83	1.2	3.7	7.5	1.5	5.9	37.5	
Bi	0.08	0.04	0.03	0.05	<0.02	0.02	0.08	<0.02	Not analyzed	<0.02	<0.02	<0.02	<0.02	0.06	0.17	
Cd	0.31	0.05	0.03	0.17	0.09	0.53	0.05	<0.01	<0.01	<0.01	0.16	<0.01	<0.01	0.07	0.22	
Co	39.9	27.8	64.1	51.9	85.8	33.2	12.5	35.8	67.6	0.5	1	1.2	1	6.2	1.8	
Cr	76.7	170.1	135.7	212.7	132.3	315.2	49.4	242.2	2580.66	5.7	8.3	7.6	7.5	21.5	3.7	
Cu	53.18	2.36	5.39	30	5.09	16.85	1.9	18.4	2.76	2.27	3.36	5.1	10.67	8.01	6.74	
Ga	1.2	0.3	0.1	0.2	0.2	1.7	0.4	4.2	3.26	<0.1	0.2	0.2	0.1	0.1	0.7	
Hg	146	11	11	<5	<5	<5	<5	<5	Not analyzed	<5	<5	12	<5	8	5	
Mo	1.62	0.12	0.14	0.31	0.05	0.44	0.42	0.37	0.033	0.33	0.42	0.36	0.34	0.4	0.69	
Ni	365.1	459.8	1344.1	1317.4	1570.3	492.7	261.3	268.5	1279.76	3.1	5.1	17.1	4	86.1	7.5	
Pb	2.56	1.72	0.81	2.73	1.69	3.76	7.92	0.37	17.43	0.06	0.23	0.31	0.15	0.87	24.59	
Sb	0.37	3.1	0.3	0.8	0.32	1.28	0.97	0.42	Not analyzed	0.14	0.12	0.17	0.12	0.58	0.62	
Sc	13.1	4.1	4.4	4.3	3.2	13.3	3.5	21.3	Not analyzed	0.2	1.1	0.7	0.6	2	0.4	
Sr	265.2	769.6	125.9	469.5	89	543.6	770.4	46.5	48.766	4.8	82.7	35.5	22.3	169.6	35.6	
Te	0.05	0.1	0.03	0.08	<0.02	0.08	0.09	<0.02	Not analyzed	0.02	<0.02	<0.02	<0.02	0.07	0.09	
Tl	0.19	0.02	<0.02	0.08	0.03	0.04	<0.02	0.04	Not analyzed	<0.02	<0.02	0.02	<0.02	<0.02	0.1	
V	54	12	5	8	3	44	8	116	29.33	<1	4	2	1	8	7	
Zn	91.2	4.9	8.7	6.8	7.1	38.7	16.6	45.6	21.33	0.5	1.8	1.1	1.1	7.7	69.8	

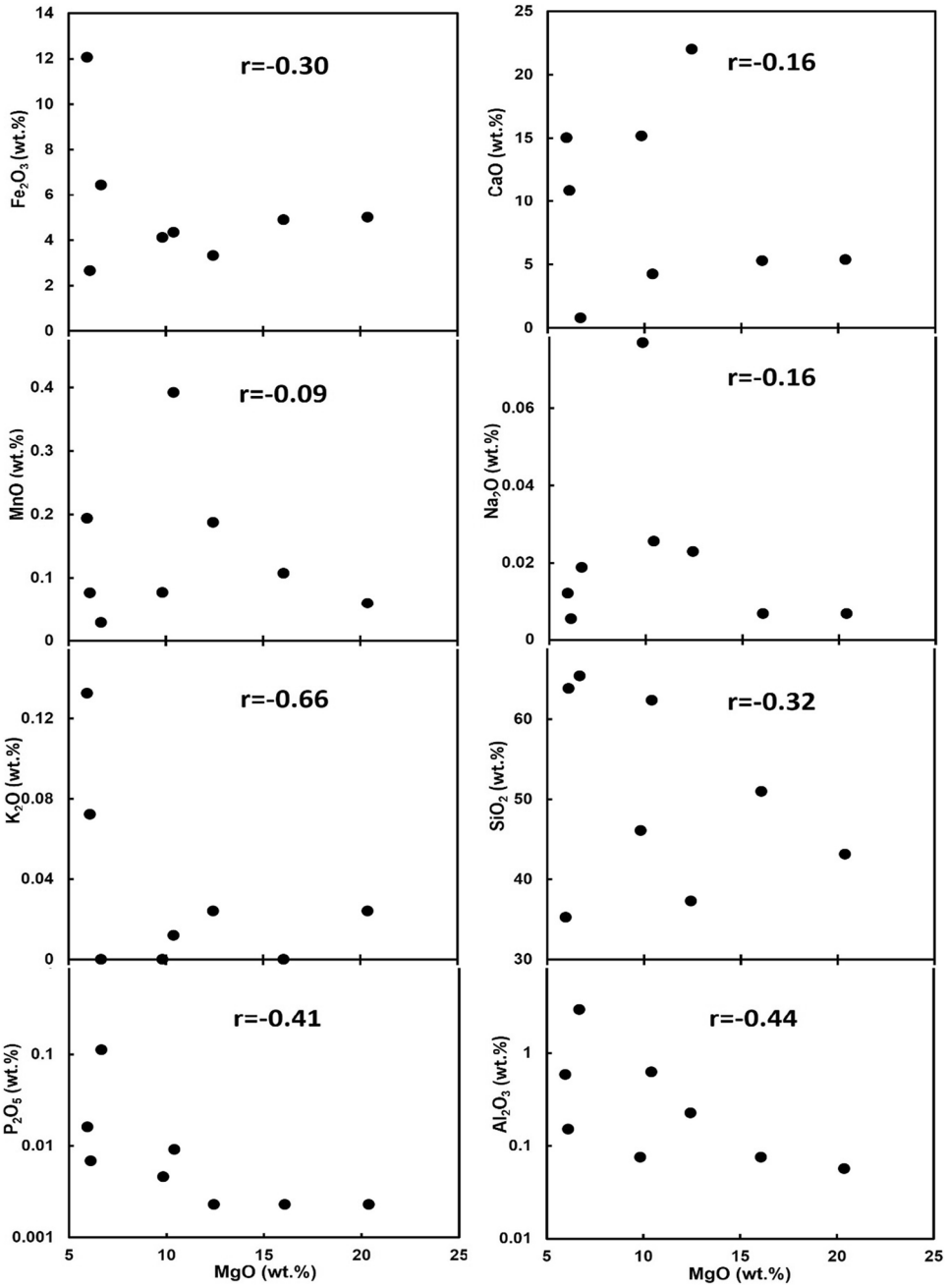

Fig. 8 Variation diagrams of MgO with some major oxides for the listvenite rocks

deformation. It is noteworthy that both high-silica listvenite and Au-bearing veins experienced more ductile deformation than low-silica listvenite.

The Spearman's rank correlation shows that gold has a positive correlation with Ag, Pb, As and Zn in the listvenite samples (Table 5). In mineralized veins, Au shows a positive correlation with Ag, Fe, Ni, As, Cu, Pb and Zn (Table 6). This is consistent with the association of free-milling gold and the late base metal sulfides (galena–tetrahedrite–arsenopyrite–chalcopyrite and pyrite assemblage). The correlations were also carried out for elements: Au, Al, Ca, Fe, Ga, K, Mg and Mn in the lode gold deposit samples. The elements related to mineralization/alteration were chosen based on their geochemical association with carbonates and other alterations, such as chloritization and sericitization of the wall rocks. In listvenite samples, Au showed a positive correlation with K and Ca (Table 7), while in mineralized quartz veins, Au has positive correlation with Ca, Mg, Mn, Fe and Al (Table 8) (Fig. 13). These results are consistent with petrographic observation that the Au-mineralization is associated with the later phase of carbonate (dolomite, ankerite, and calcite), chlorite and fuchsite formation.

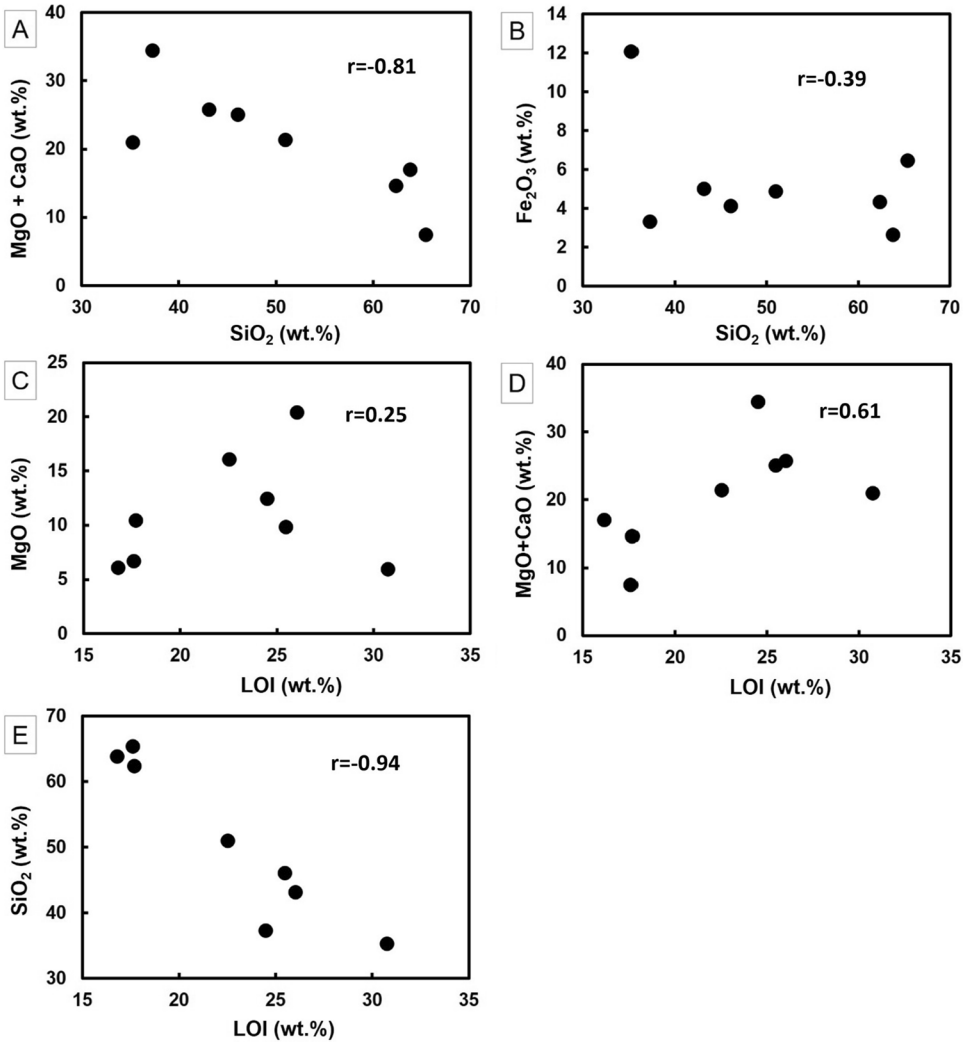

Fig. 9 Bivariate plots: **A**, **B** SiO_2 versus MgO + CaO, and Fe_2O_3. **C**–**E** Loss of ignition (LOI) versus MgO, MgO + CaO, and SiO_2 of listvenite

Rare earth elements

In the high- and low-silica listvenites, REE-normalized patterns show minor enrichment in LREE relative to HREE compared to serpentinite, with a LREE/HREE ratio of 1.7–3.2, with an average of 2.34, and $(La/Yb)_N$ of 2.8–13.8, with average of 6.2 (Fig. 8A).

The REE normalized pattern of gold-bearing quartz vein displays a steep, negatively sloping LREE pattern, flat HREE pattern, and strongly negative Eu anomaly (Fig. 14A). In the lode gold mineralization of El-Barramiya area, highly fractionated LREE (LREE/HREE ratio = 10.7 and $(La/Yb)_N = 27.4$) and depletion in HREE (Fig. 13A) relative to the serpentinite host rocks and listvenites may be due to the existence of phases other than quartz-bearing carbonates and wall rock material. Zoheir (2008) and Zoheir et al. (2013) suggest dominant metamorphic water, with possible contributions from a magmatic source. This may provide an internal fluid supply (dehydration of the metasedimentary and metavolcanic rocks) through the region's peak metamorphism in the area. The occurrence of strongly negative Eu anomaly in both listvenites and hydrothermal quartz vein (Fig. 14A) could be related to highly acid pH conditions and/or an increase in fO_2 of the hydrothermal system (Sverjensky 1984; Bau 1991). The average primitive mantle-normalized trace element pattern (normalization values of McDonough and Sun 1995) of each rock variety studied is shown in (Fig. 14B). Generally, all the patterns show slight to moderate enrichment in large ion lithophile elements (Rb and Sr, Th) and relative depletion in high field strength elements (Zr and Pb) and REEs.

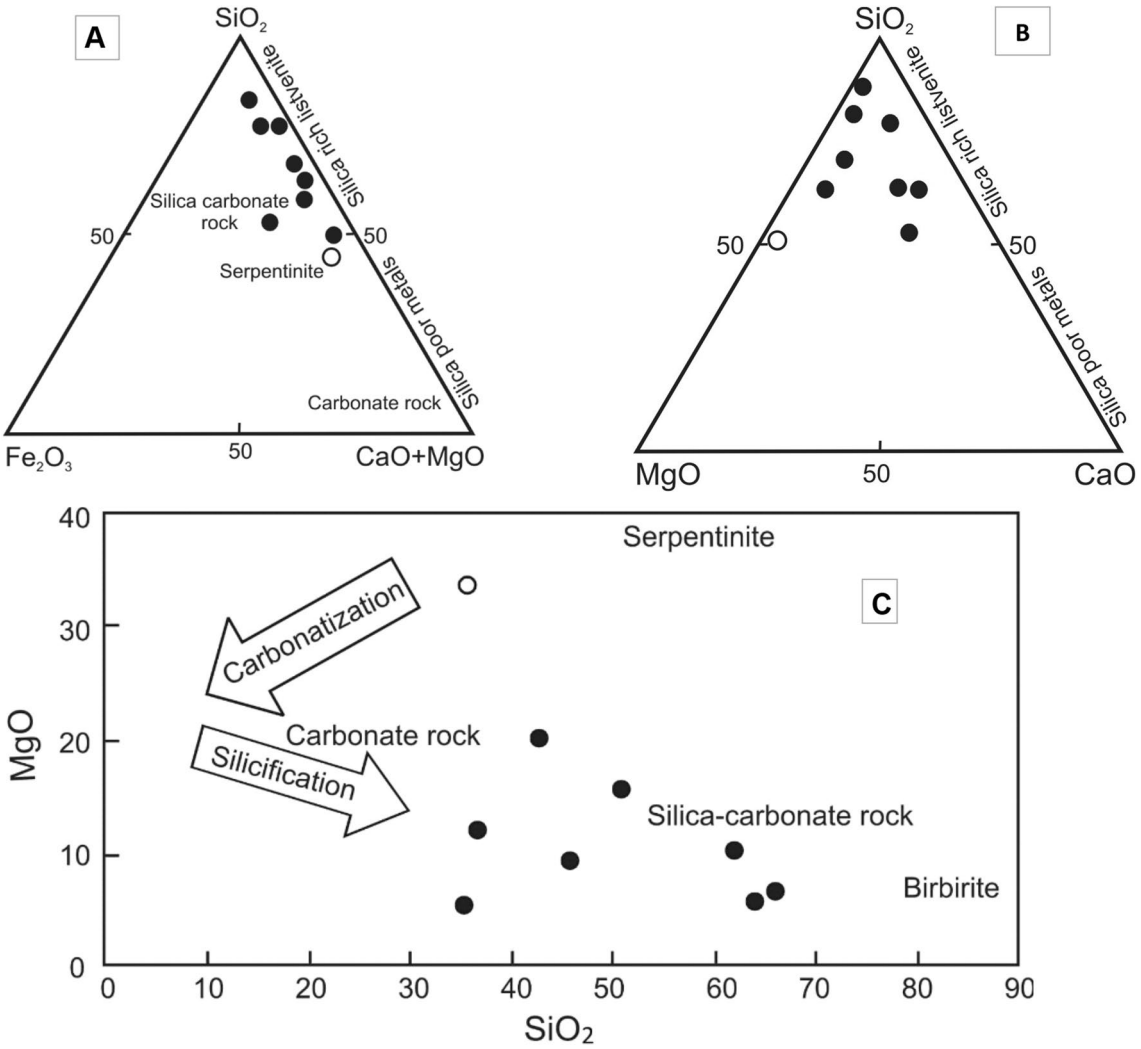

Fig. 10 **A** Fe_2O_3–SiO_2–MgO + CaO ternary diagram with alteration trends of serpentinites and fields of altered rocks according to Akbulut et al. (2006). **B** MgO–SiO_2–CaO ternary diagram. **C** SiO_2 versus MgO binary diagram (wt%) shows chemical changes during alteration of serpentinites, according to Akbulut et al. (2006). Solid circles represent listvenite rocks and empty circle represents an average of serpentinites

Discussion

El-Barramiya lode gold mineralization is occupied in a zone of strongly sheared ophiolitic rocks trending ENE. It is hosted by an ophiolitic mélange consisting of allochthonous blocks of serpentinites and listvenite structurally intercalated with metasedimentary and volcano-sedimentary rocks. Quartz and quartz-carbonate veins as well as altered wall rocks (listvenite) make up the mineralization. Sulfide minerals associated with gold in the quartz-carbonate veins and adjacent listvenite are arsenopyrite, pyrite and trace amounts of chalcopyrite, sphalerite, tetrahedrite, pyrrhotite, galena and gersdorffite. The geologic characteristics of the Barramiya deposit; its structural control, host rocks, alteration mineralogy, mineralization style, timing of the mineralization with respect to the deformation history, along with the fluid and stable isotope data, are in accordance with the orogenic mesothermal lode-gold deposit style in the sense of Groves et al. (2003), analogous to other deposits in the Eastern Desert (e.g., Helmy et al. 2004; Zoheir 2008; Zoheir and Lehmann. 2011).

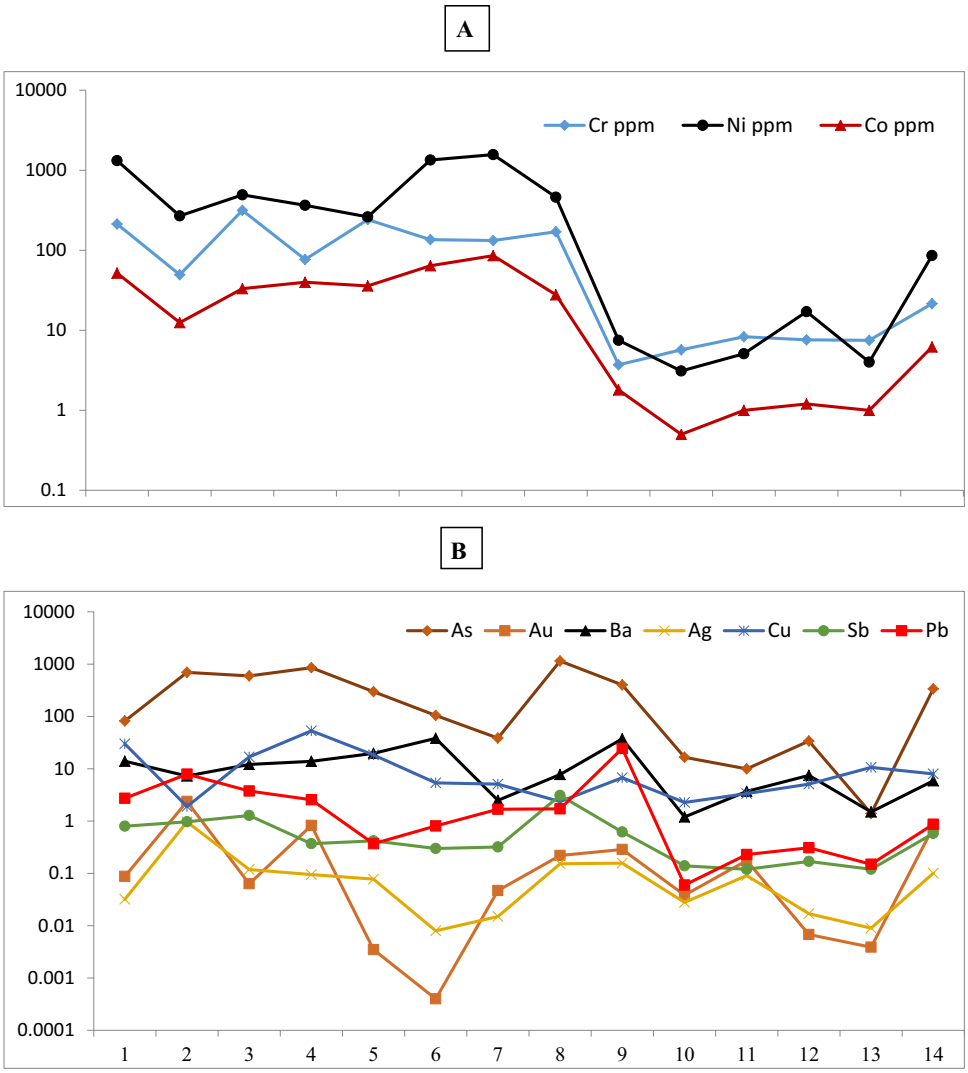

Figs. 11 **A** Co, Ni, Cr element distributions in Listvenites: (1–8) and Quartz Veins (9–14), **B** trace element distributions in all listvenite samples ($n=8$) and quartz vein samples ($n=6$) for Au, As, Ba, Ag, Cu, Sb and Pb elements

Gold-bearing quartz and quartz-carbonate veins as well as listvenite from El-Barramiya area contain low salinity (~ 4 wt% NaCl eq.) aqueous (H_2O) and mixed H_2O–$CO_2 \pm CH_4$ fluid inclusions. Petrographic investigation and microthermometry (total homogenization temperatures and the variable CO_2 densities) suggest heterogeneous trapping of these fluids after phase separation. Metamorphism produces large quantities of CO_2 and produces carbonate-rich sedimentary rocks (Goldfarb et al. 2017). Generally, carbonaceous shale is a suitable source rock for elements that are commonly enriched in orogenic gold deposits, such as S, Au, As, and Sb (Large et al. 2011; Lisitsin and Pitcairn 2016; Pitcairn 2011; Steadman et al. 2014). These may also account for the deposition of sulfides associated with gold mineralization in El-Barramiya area. El-Barramiya gold-bearing veins and wall rocks are situated in carbonaceous listvenite rocks and associated with arsenopyrite, pyrite and pyrrhotite, and to lesser extent sphalerite and galena mineralizations. This proves that gold was transported as gold bisulfide ($Au(HS)_2^-$) complexes. The fluid inclusions study indicates that the heterogeneous trapping of mineralized fluids were low salinity aqueous-carbonic. According to Naden and Shepherd (1989) and Shepherd et al. (1991) contamination of CO_2-bearing fluids by reaction with rocks containing carbonaceous matter is widely invoked to explain the presence of CH_4 and N_2 in fluid inclusions from shear zone-hosted gold deposits. Decreasing in fO_2 of the fluid may due to the addition of CH_4 during fluid–rock carbon interaction and carbonate precipitation. Consequently, destabilized gold–sulfur complexes, with sulfur consumption by sulfidation can lead to gold deposition. Refractory gold in early sulfide assemblage was deposited from a low-salinity $CO_2 \pm CH_4$–H_2O–NaCl or H_2O–NaCl–$CO_2 \pm CH_4$ fluid concomitant with the arsenopyrite + pyrite + pyrrhotite ± gersdorffite assemblage, whereas, the free-milling gold could have been mobilized and redistributed during deformation (Zoheir and Lehmann 2011).

Table 4 Rare earth elements composition of the listvenite, serpentinites and quartz veins of El-Barramiya area (ppb)

Sample no.	Listvenite						Quartz vein	Serpentinites
	1	2	4	6	7	8	14	($n=3$)
La	4.3	0.5	1	0.5	0.9	0.5	13.2	11.4
Pr	1.25	0.02	0.33	0.13	0.3	0.02	2.52	3.29
Nd	5.87	0.06	2.08	0.92	1.38	0.07	9.56	14.2
Sm	1.89	< 0.02	0.8	0.32	0.62	< 0.02	1.7	3.9
Eu	0.49	< 0.02	0.62	0.13	0.15	< 0.02	0.42	1.08
Gd	2.37	< 0.02	0.96	0.37	0.68	0.04	1.25	4.48
Tb	0.24	< 0.02	0.14	0.05	0.08	< 0.02	0.18	0.71
Dy	1.02	< 0.02	0.68	0.18	0.34	< 0.02	0.63	4.86
Ho	0.14	< 0.02	0.13	0.05	0.06	< 0.02	0.09	1.03
Er	0.33	< 0.02	0.4	0.13	0.15	< 0.02	0.22	2.96
Tm	0.03	< 0.02	0.06	0.02	0.023	< 0.02	0.02	0.4
Yb	0.26	0.02	0.37	0.12	0.13	0.02	0.17	2.68
Lu	0.03	< 0.02	0.05	0.014	0.02	< 0.02	0.01	0.38
∑ REE	18.22	0.6	7.62	2.9	4.79	0.65	29.97	51.37
∑ LREE	13.8	0.58	4.83	2	3.35	0.59	27.4	33.87
∑ HREE	4.42	0.02	2.79	0.9	1.44	0.06	2.57	17.5
∑LREE/∑ HREE	3.1	29	1.7	2.2	2.3	9.83	10.7	1.9
La/Yb	11.1	25	1.8	2.8	4.7	25	52.3	2.8

$Eu/Eu^{*}=Eu_n/\sqrt{(Sm_n \times Gd_n)}$, $La_N/Yb_N=(La/La_N)/(Yb/Yb_N)$, $La_N/Sm_N=(La/La_N)/(Sm/Sm_N)$, $Sm_N/Yb_N=(Sm/Sm_N)/(Yb/Yb_N)$

Vearncombe and Zelic (2015) evaluated the relationship between structural discontinuities (faults, shear zones, fold noses, competency contrasts) and the production of orogenic gold deposits. These discontinuities serve as conduits for fluid migration from the metamorphic dehydration zone below the transition from green schist to amphibolite to the precipitation site in the upper crust, which is frequently in the greenschist facies. A dextral shear system that formed in the area's late deformation history is geographically and temporally connected to the gold-bearing quartz (± carbonate) veins (Zoheir and Lehmann 2011). Petrographic study illustrated that El-Barramiya area was subjected to hydrothermal metasomatic alteration processes (carbonatization and silicification). Listvenite is the result of metasomatic alteration of serpentinites. Geochemical study of listvenite exhibited higher levels of As, Sb and Hg which suggests the contribution of granite-related hydrothermal fluids; whereas the presence of Cr, Ni, Co and Pt points to the ultramafic protolith (Likhoidov et al. 2007). In El-Barramiya area, low grade green schist metamorphic, petrographic observations, such as the co-existing of actinolite and chlorite in the peak assemblage, indicate that the metamorphism was reached at the greenschist–amphibolite facies transition. Abu-Alam and Hamdy (2014) suggest metamorphic conditions of upper greenschist facies (e.g. 300–400 °C) for the ophiolitic rocks of the Arabian–Nubian Shield.

The primitive mantle-normalized trace element patterns of an average serpentinites, high and low silica listvenites are shown in (Fig. 14B). In general, all the patterns exhibit a relative depletion of high field strength elements (Zr and Pb) and REEs and a modest to moderate enrichment in big ion lithophile elements (Rb and Sr). In the study area, there is a spatial association of gold-bearing quartz ± carbonate veins and listvenite along a transecting network of steeply dipping faults, shear zones and fractures adjacent to granodiorite.

Conclusions

Ophiolitic rocks in the El-Barramiya area of the Eastern Desert, Egypt, were subjected to carbonatization and silicification metasomatic alterations. Intense alteration allowed listvenite formation in gold-bearing shear zones. The gold-bearing quartz (± carbonate) veins are spatially and temporally linked to a dextral shear system developed in the late stages of the deformation history of the area. Presence of massive to heavily asymmetric and deformed microstructures, dynamic recrystallization and slip on discrete carbonaceous laminae indicate that formation of mineralized quartz veins under variable compressional and tensional regimes.

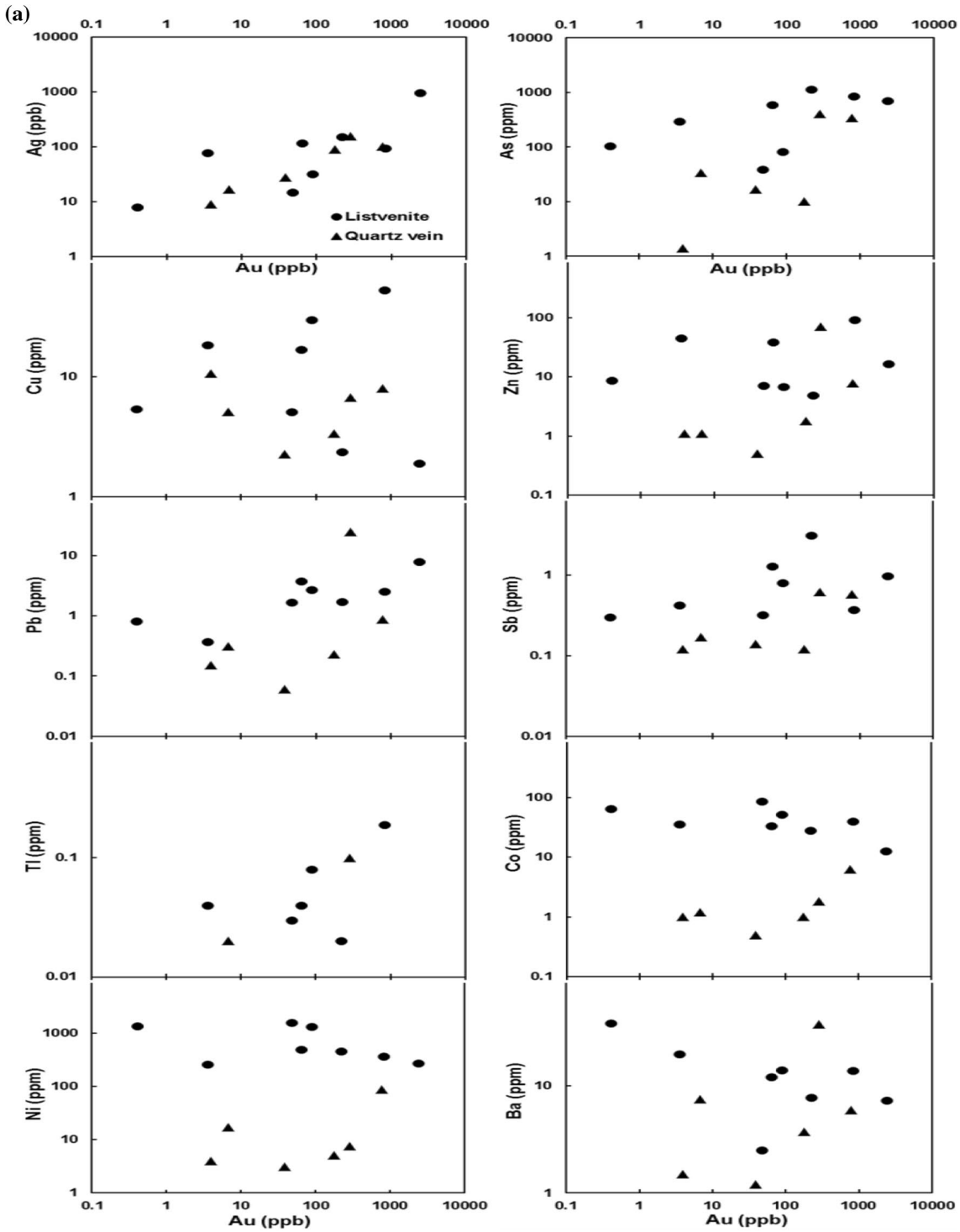

Fig. 12 **A** Bivariate plots of Au versus other trace elements of the listvenite (solid circular samples) and quartz veins samples (triangular samples). **B** Bivariate plots of Ag versus other trace elements of the (solid circular samples) and quartz veins samples (triangular samples)

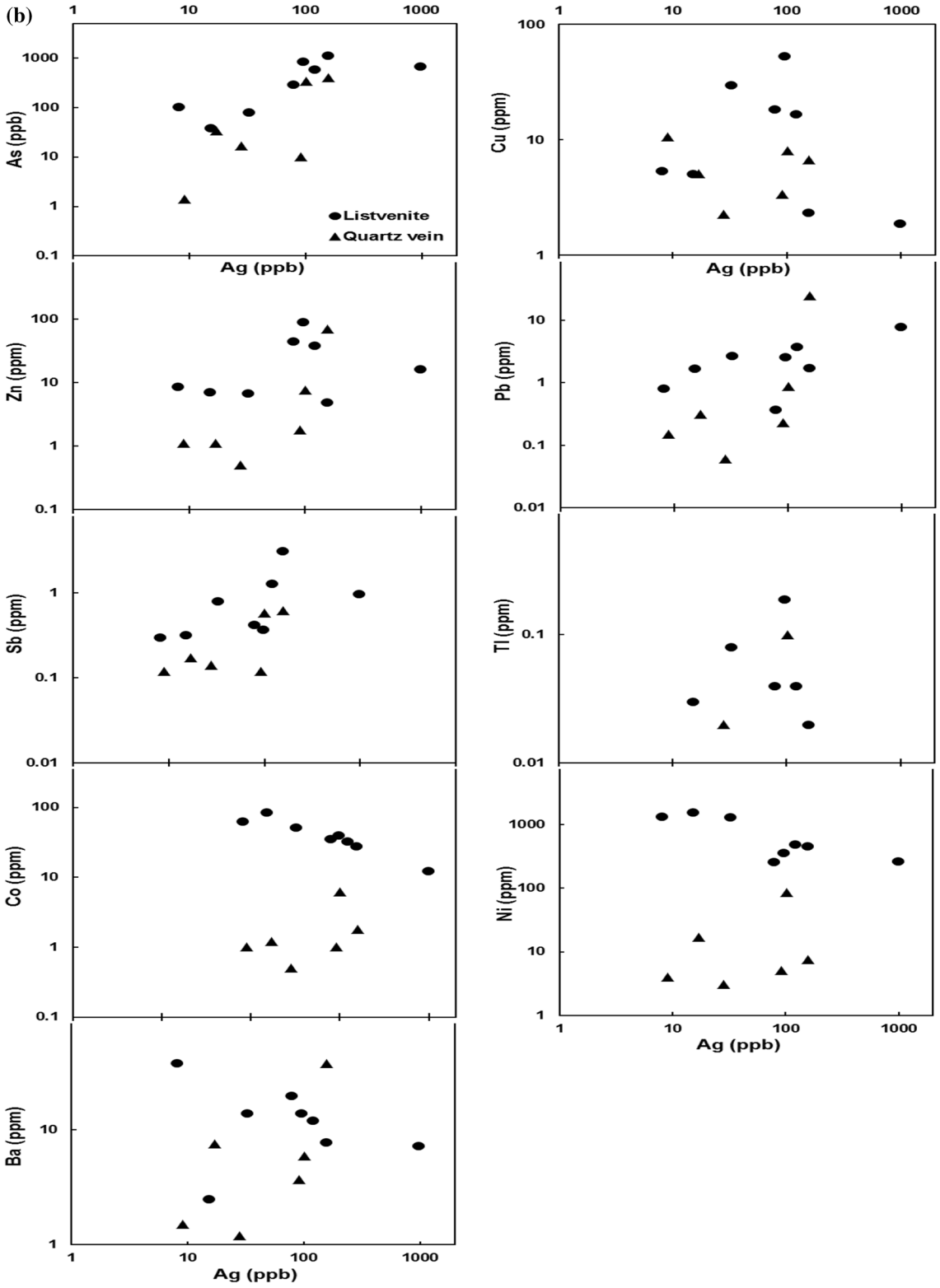

Fig. 12 (continued)

Table 5 Spearman's correlation coefficients for listvenite samples from El-Barramiya lode-gold deposit

Element	Au	Ag	Cu	Fe	Ni	As	Zn	Pb	Cr
Ag	0.95								
Cu	− 0.07	− 0.31							
Fe	− 0.09	− 0.35	0.84						
Ni	− 0.47	− 0.48	− 0.18	− 0.2					
As	0.39	0.35	0.09	0.12	− 0.75				
Zn	0.11	− 0.09	0.8	0.89	− 0.55	0.33			
Pb	0.88	0.9	− 0.13	− 0.31	− 0.35	0.31	− 0.03		
Cr	− 0.67	− 0.49	− 0.01	− 0.21	− 0.01	− 0.17	− 0.06	− 0.36	
Co	− 0.6	− 0.66	− 0.02	0.11	0.89	− 0.73	− 0.25	− 0.57	0.01

Table 6 Spearman's correlation coefficients for mineralized veins samples from El-Barramiya lode-gold deposit

Element	Au	Ag	Cu	Fe	Ni	As	Zn	Pb	Cr
Ag	0.62								
Cu	0.24	− 0.01							
Fe	0.83	0.85	0.06						
Ni	0.9	0.26	0.3	0.63					
As	0.76	0.83	0.29	0.8	0.54				
Zn	0.21	0.79	0.14	0.49	− 0.01	0.77			
Pb	0.14	0.76	0.12	0.44	− 0.16	0.73	0.99		
Cr	0.83	0.11	0.3	0.51	0.95	0.33	− 0.03	− 0.03	
Co	0.95	0.41	0.38	0.72	0.98	0.67	0.06	− 0.01	0.92

Table 7 Spearman's correlation coefficients for listvenite samples from El-Barramiya lode-gold deposit

Element	Au	Ca	Al	Fe	K	Mg	Mn
Ca	0.1						
Al	− 0.21	− 0.49					
Fe	− 0.09	− 0.08	0.27				
K	0.51	− 0.06	0.3	0.77			
Mg	− 0.5	− 0.14	− 0.47	− 0.05	− 0.44		
Mn	− 0.13	0.64	− 0.19	0.07	− 0.23	− 0.05	
Ga	− 0.19	− 0.41	0.97	0.3	0.16	− 0.51	− 0.01

Table 8 Spearman's correlation coefficients for mineralized veins samples from El-Barramiya lode-gold deposit

Element	Au	Ca	Al	Fe	K	Mg	Mn
Ca	0.95						
Al	0.22	0.12					
Fe	0.83	0.87	0.54				
K	− 0.04	− 0.03	0.99	0.31			
Mg	0.83	0.92	− 0.25	0.66	− 0.66		
Mn	0.83	0.93	0.28	0.94	− 0.28	0.82	
Ga	− 0.02	− 0.14	0.97	0.37	0.98	− 0.5	0.05

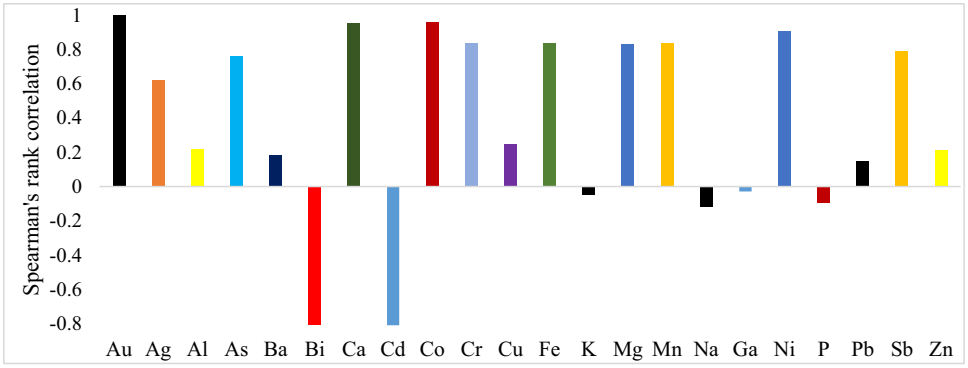

A) Spearman's rank correlation in Quartz.

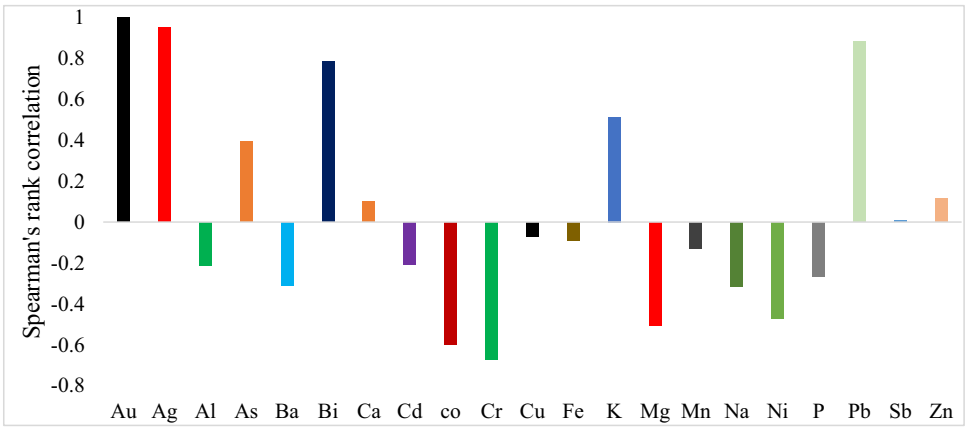

B) Spearman's rank correlation in Listvenite.

Fig. 13 Histgram showing Speaman's rank correlation in lode gold deposits from El-Barramiya area

The frequent association of orogenic gold deposit with various sulfides (e.g. pyrite, arsenopyrite and pyrrhotite) suggests the role of sulfidation process in transportation and deposition of gold in the study area. Graphite schist and serpentinites are a suitable source rocks for elements that are commonly enriched in orogenic gold deposits such as S, Au, As and Sb. Fluid-graphite schist reactions and carbonate precipitation are likely resulted in destabilizing gold–sulfur complexes and the coexisting sulfidation process triggered gold deposition.

Fluid inclusions study suggests a heterogeneous trapping of low-salinity aqueous-carbonic fluid $\pm CH_4$ after phase separation. The minimum *P–T* conditions of fluid inclusions trapping as well as gold deposition were estimated between 280 and 340 °C, and pressure between 1.5 kbar and 1.9 kbar, which is consistent with the mesothermal conditions.

Geochemical study of listvenite and mineralized veins demonstrated that high trace element concentrations such as Co, Cr, Ni and V in listvenite confirm the ultramafic genesis. Also, the random distribution for the elements Au, Ag, Cu, Sb, As, Rb, Ba and Zn reflects the effect of the hydrothermal fluids. Highly, more fractionated LREE and depletion in HREE of gold-bearing quartz vein relative to the serpentinites host rocks and listvenite can be attributed to the presence of other phases affecting the formation of quartz carbonates veins and gold-bearing wall rocks. This phase may be considered as the contribution of granitic intrusions in the geochemical characterization.

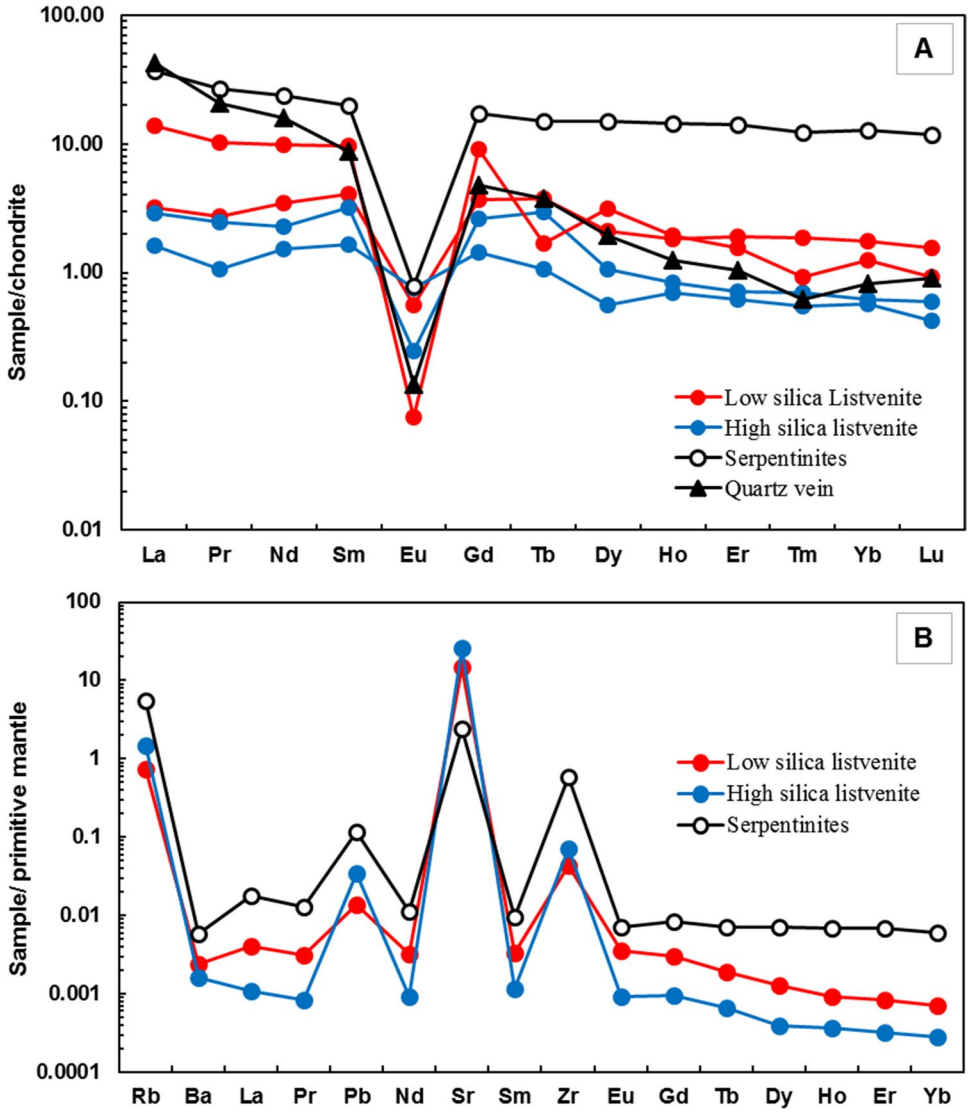

Fig. 14 **A** Chondrite-normalized REE patterns for listvenite, quartz vein and an average of serpentinites ($n=3$ samples) (Boynton 1984). **B** Primitive mantle-normalized spider diagrams for an average of listvenites and serpentinites, normalization values from McDonough and Sun (1995)

Acknowledgments The author is grateful to Professor Richard Palin (Oxford University, United Kingdom) for his helpful review and to thanks reviewers for their helpful reviews

Author contributions The authors on this paper include MA, HE, MA, AS agree to publish the article.

Funding Open access funding provided by The Science, Technology & Innovation Funding Authority (STDF) in cooperation with The Egyptian Knowledge Bank (EKB). The authors have not disclosed any funding.

Data Availability The authors confirm that the data supporting the findings of this study are available within the article and its supplementary material. Raw data that support the findings of this study area available from the corresponding author upon responsible request.

Declarations

Conflict of interest The authors declare that there is no conflict of interest.

References

Abdel-Karim A-AM, et al. (2017) Mineral chemistry and geochemistry of ophiolitic ultramafics from central Eastern Desert, Egypt: a case for contaminated mantle-derived magma. EGU General Assembly Conference Abstracts

Abdel-Karim AAM, Ali S, El-Shafei SA (2018) Mineral chemistry and geochemistry of ophiolitic metaultramafics from Um Halham and Fawakhir, Central Eastern Desert, Egypt. Int J Earth Sci 107:2337–2355

Abdel-Khalek ML (1979) Tectonic evolution of the basement rocks in the southern and central Eastern Desert of Egypt, Evolution and Mineralization of the Arabian-Nubian Shield, 1 AMS Al-Shanti, 53–62. Pergamon, Elmsford

Abdelrady M et al. (2023) Geophysical investigations for the identification of subsurface features influencing mineralization zones. J King Saud Univer Sci, 102809

Abu-Alam TS, Hamdy MM (2014) Thermodynamic modelling of Sol Hamed serpentinite, South Eastern Desert of Egypt: implication for fluid interaction in the Arabian-Nubian Shield ophiolites. J Afr Earth Sc 99:7–23

Akbulut M, Pïşkïn Ö, Karayïğït Aİ (2006) The genesis of the carbonatized and silicified ultramafics known as listvenites: a case study from the Mihaliççik region (Eskişehir). NW Turkey. Geol J 41(5):557–580

Bau M (1991) Rare-earth element mobility during hydrothermal and metamorphic fluid rock interaction and the significance of the oxidation state of europium. Chem Geol 93:219–230

Boynton WV (1984) Cosmochemistry of the rare earth elements: meteorite studies. Develop Geochem Elsevier 2:63–114

Brown PE (1989) Flincor, A microcomputer program for the reduction and investigation of fluid inclusion data. Am Miner 74:1390–1393

Brown PE, Lamb WM (1989) P-V–T properties of fluids in the system H_2O–CO_2–NaCl: new graphical presentations and implications for fluid inclusion studies. Geochim Cosmochim Acta 53:1209–1221

Buisson G, Leblanc M (1986) Gold-bearing listwaenites (carbonatized ultramafic rocks) from ophiolite complexes. In: Conference metallogeny of basic and ultrabasic rocks

Buryak VA (1982) Metamorphism and ore formation. Nedra, Moscow **(256 pp., in Russian)**

Buryak VA, Khmelevskaya NM (1997) Sukhoi log as one of the largest gold deposits in the world: genesis, distribution patterns, prospecting criteria. Dalnauka, Vladivostok **(156 pp., in Russian)**

Chen J (2006) Orogenic-type deposits and their metallogenic model and exploration potential. Geol China 33:1181–1196

Cox SF, Etheridge MA, Wall VJ (1987) The role of fluids in syntectonic mass transport, and the localization of metamorphic vein-type ore deposits. Ore Geol Rev 2:65–86

Decrausaz T, Godard M, Menzel MD, Parat F, Oliot E, Lafay R, Barou F (2023) Pervasive carbonation of peridotite to listvenite (Semail Ophiolite, Sultanate of Oman): clues from iron partitioning and chemical zoning. Eur J Mineral 35:171–187. https://doi.org/10.5194/ejm-35-171-2023

Diamond LW (1992) Stability of CO_2 clathrate hydrate + CO_2 liquid + CO_2 vapour + aqueous KCl-NaCl solutions: experimental determination and application to salinity estimates of fluid inclusions. Geochim Cosmochim Acta 56:273–280

El-Gaby S, List FK, Tehrani R (1988) Geology, evolution and metallogenesis of the Pan-African belt in Egypt. In: El-Gaby S, Greiling RO (eds) The Pan-African belt of Northeast Africa and adjacent areas. Vieweg and Sohn, Braunschneig, pp 17–68

Fall A, Tattitch B, Bondar RJ (2011) Combined microthermometric and Raman spectroscopic technique to determine the salinity of H_2O–CO_2–NaCl fluid inclusions based on clathrate melting. Geochim Cosmochim Acta 75:951–964

Fowler A, Osman AF (2009) The Sha'it–Nugrus shear zone separating Central and South Eastern Deserts, Egypt: A post-arc collision low-angle normal ductile shear zone. J African Earth Sci 53(1–2):16–32

Gahlan HA, Azer MK, Asimow PD, Al-Kahtany KM (2020a) Petrogenesis of gold-bearing listvenites from the carbonatized mantle section of the neoproterozoic Ess ophiolite, Western Arabian Shield, Saudi Arabia. Lithos 372–373:105679

Gahlan HA, Azer MK, Asimow PD, Al-Kahtany KM (2020b) Petrogenesis of goldbearing listvenites from the carbonatized mantle section of the neoproterozoic Ess ophiolite, western arabian shield, Saudi Arabia. Lithos 12:105679

Gahlan HA, Azer MK, Asimow PD, Al-Kahtany KM (2022) Formation of gold-bearing listvenite in the mantle section of the Neoproterozoic Bir Umq ophiolite, Western Arabian Shield, Saudi Arabia. J Afr Earth Sc 190:1464–2343

Goldfarb RJ, Groves DI, Gardoll S (2001) Orogenic gold and geologic time: a global synthesis. Ore Geol Rev 18:1–75

Goldfarb RJ, Mayer ASA, Jowitt SM, Mudd GM (2017) West Africa: the world's premier Paleoproterozoic gold province. Econ Geol 112:123–143

Goncharenko A (1970) Auriferous listwanites as a new type of mineralization in the northern part of the Kuznetsk Alatau. Izvestiya Tomskogo Politekhnicheskogo Instituta Rep Tomsk Polytech Inst 239:110–114

Groves D (1993) The crustal continuum model for late-Archaean lode-gold deposits of the Yilgarn Block, Western Australia. Miner Depos 28:366–374

Groves DL, Goldfarb RJ, Gebre-Mariam M, Hagemann SG, Robert F (1998) Orogenic gold deposits: a proposed classification in the context of their crustal distribution and relationship to other gold deposit types. Ore Geol Rev 13:7–27

Groves DI, Goldfarb RJ, Robert F, Hart CJR (2003) Gold deposits in metamorphic belts: overview of current understanding, outstanding problems, future research, and exploration significance. Econ Geol 98(1):1–29

Hansen LD, Dipple GM, Gordon TM, Kellett DA (2005) Carbonated serpentinite (listwanite) at Atlin, British Columbia: a geological analogue to carbon dioxide sequestration. Can Mineral 43:225–239

Helmy HM, Kaindle R, Fritz H, Loizenbauer J (2004) The Sukari Gold Mine, Eastern Desert—Egypt: structural setting, mineralogy and fluid inclusion study. Miner Depos 39(4):495–511

Kuleshevich L (1984) Listvenity v zelenokamennykh poyasakh vostochnoj Karelii. Geol Rudnyh Mestorožděnij 26(3):112–116

Large RR, Bull SW, Maslennikov VV (2011) A carbonaceous sedimentary source rock model for Carlin-type and orogenic gold deposits. Econ Geol 106:331–358

Likhoidov G, Plyusnina LP, Shcheka ZA (2007) The behavior of gold during listvenitization: Experimental and theoretical simulation. Doklady Earth Sciences, Springer Nature BV, New York

Lisitsin VA, Pitcairn IK (2016) Orogenic gold mineral systems of the Western Lachlan Orogen (Victoria) and the Hodgkinson Province (Queensland): crustal metal sources and cryptic zones of regional fluid flow. Ore Geol Rev 76:280–295

Mahmoud MMA (2013) Geological and geophysical studies of El-Barramiya Gold Mine Area, Eastern Desert, Egypt. M.sc. thesis, Faculty of Science, Assiut University

McDonough WF, Sun SS (1995) The composition of the Earth. Chem Geol 120(3–4):223–253

Mohamed A, Abdelrady M, Alshehri F, Mohammed MA, Abdelrady A (2022) Detection of mineralization zones using aeromagnetic data. Appl Sci 12:9078

Moussa HE, Azer MK, Abou El Maaty MA, Maurice AE, Yanni NN, Akarish AI, Elnazer AA, Elsagheer MA (2021) Carbonation of Neoproterozoic mantle section and formation of gold-bearing listvenite in the Northern Nubian Shield. Lithos 406(407):106525

Naden J, Shepherd TJ (1989) Role of methane and carbon dioxide in gold deposition. Nature 342:793–795

Osman A (2014) An integrated metallotect and petrographic model for gold mineralization in the Eastern Desert of Egypt; a new prospecting vision. Egypt J Pure Appl Sci 52:41–54

Pirajno F (2009) Hydrothermal processes and mineral systems. Geological Survey of Western Australia. Springer, Berlin

Pitcairn I (2011) Background concentrations of gold in different rock types. Appl Earth Sci 120:31–38

Pohl W (1988) Precambrian metallogeny of NE-Africa. The Pan-African belt of Northeast Africa and adjacent areas: tectonic evolution and economic aspects of a late Proterozoic orogen, pp 319–341

Saleh A, Abdelmoneim M, Abdelrady M, Al Deep M (2018) Subsurface structural features of the basement complex and mineralization zone investigation in the Barramiya area, Eastern Desert of Egypt, using magnetic and gravity data analysis. Arab J Geosci 11:1–14

Shalaby A, Stüwe K, Makroum F, Fritz H, Kebede T, Klötzli U (2005) The Wadi Mubarak belt, Eastern Desert of Egypt: a Neoproterozoic conjugate shear system in the Arabian-Nubian Shield. Precambr Res 136:27–50

Shepherd T, Bottrell SH, Miller MF (1991) Fluid inclusion volatiles as an exploration guide to black shale-hosted gold deposits, Dolgellau gold belt, North Wales, UK. J Geochem Explor 42:5–24

Steadman JA, Large RR, Davidson GJ, Bull SW, Thompson J, Ireland TR, Holden P (2014) Paragenesis and composition of ore minerals in the Randalls BIF-hosted gold deposits, Yilgarn craton, Western Australia: implications for the timing of deposit formation and constraints on gold sources. Precambr Res 243:110–132

Stern RJ, Hedge CE (1985) Geochronologic and isotopic constraints on Late Precambrian crustal evolution in the Eastern Desert of Egypt. Am J Sci 2285:97–127

Sverjensky DA (1984) Europium redox equilibrium in aqueous solution. Earth Planet Sci Lett 67:70–78

Vearncombe J, Zelic M (2015) Structural paradigms for gold: do they help us find and mine? Appl Earth Sci 124:2–19

Zhang YG, Frantz JD (1987) Determination of the homogenization temperature and densities of supercritical fluids in the system NaCl-KCl-CaCl2-H2O using synthetic fluid inclusions. Chem Geol 64:335–350

Zoheir BA (2008) Characteristics and genesis of shear zone-related gold mineralization in Egypt: a case study from the Um El Tuyor mine, south Eastern Desert. Ore Geol Rev 34:445–470

Zoheir B, Lehmann B (2011) Listvenite–lode association at the Barramiya gold mine, Eastern Desert. Egypt Ore Geol Rev 39:101–115

Zoheir B, Abdel-Fattah MG, El-Alfy SM (2013) Geochemistry and mineral chemistry of lode gold mineralisation, SE Egypt: implications for ore genesis and exploration. Arab J Geosci 6:4635–4646

Zoheir BA, Johnson PR, Goldfarb RJ, Klemm DD (2019) Orogenic gold in the Egyptian Eastern Desert: widespread gold mineralization in the late stages of Neoproterozoic orogeny. Gondwana Res 75:184–217

Zoheir BA, Weihed P (2014) Greenstone-hosted lode-gold mineralization at Dungash mine, Eastern Desert Egypt. J African Earth Sci 99:165–187

Authors and Affiliations

Mohamed Abdelrady[1] · Hany Elhadek[1] · Mohamed Abdelmoneim[1] · Ahmed Saleh[2]

✉ Mohamed Abdelrady
mohamed.abdelrady@aun.edu.eg

Hany Elhadek
hany_elhadek@yahoo.co.uk

Mohamed Abdelmoneim
m_moneim58@yahoo.com

Ahmed Saleh
ahmedsnnus@yahoo.com

[1] Geology Department, Faculty of Science, Assiut University, Assiut 71516, Egypt

[2] National Research Institute of Astronomy and Geophysics, Helwan, Cairo 11421, Egypt